Cell Reports
Medicine

Article

Single-Cell Analyses Identify Dysfunctional CD16^{+} CD8 T Cells in Smokers

Graphical Abstract

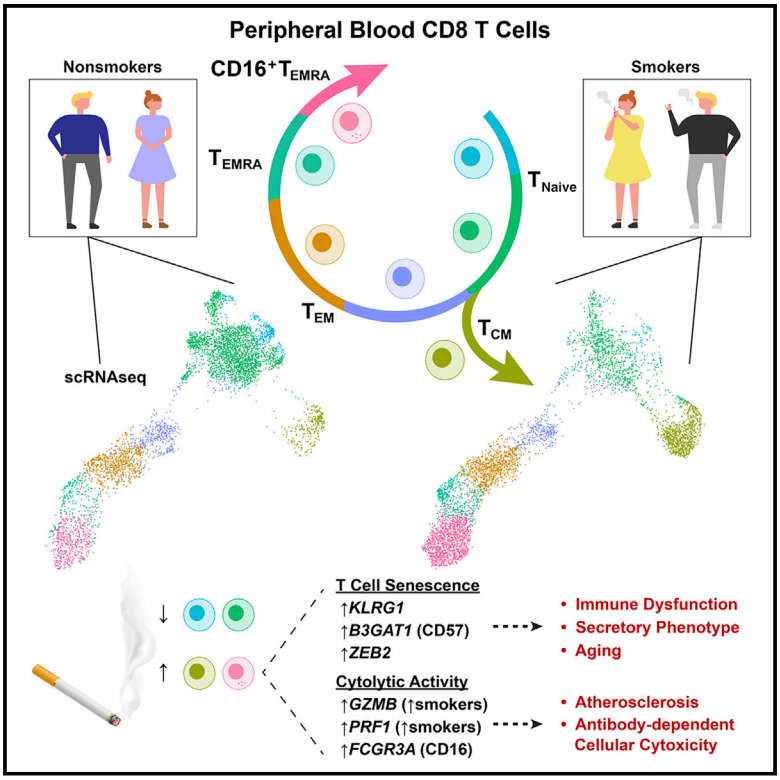

Highlights

- Smoking shifts the composition of CD8 T cells from naive to differentiated states
- NK-like CD16^{+} CD8 T_{EMRA} cells are elevated in smokers and express *GZMB* and *PRF1*
- DNA methylation links smoking dose with age acceleration and shortened telomeres
- CD8 T, CD4 T, NKT, NK, and monocytes express senescence-linked genes in smokers

Authors

Suzanne N. Martos, Michelle R. Campbell, Oswaldo A. Lozoya, ..., Ma Wan, Gary S. Pittman, Douglas A. Bell

Correspondence

bell1@niehs.nih.gov

In Brief

Smoking increases the risk of inflammatory diseases and decreases immunity. Martos et al. characterize immune cells and find that smoking reduces naive and increases late-stage CD8 T cells. They show that smoking dose is associated with age acceleration and shortened telomeres. These changes are consistent with immune aging and senescence.

Martos et al., 2020, Cell Reports Medicine *1*, 100054
July 21, 2020
https://doi.org/10.1016/j.xcrm.2020.100054

Cell Reports Medicine

CellPress
OPEN ACCESS

Article

Single-Cell Analyses Identify Dysfunctional CD16$^+$ CD8 T Cells in Smokers

Suzanne N. Martos,[1,3] Michelle R. Campbell,[1,3] Oswaldo A. Lozoya,[1] Xuting Wang,[1] Brian D. Bennett,[2] Isabel J.B. Thompson,[1] Ma Wan,[1] Gary S. Pittman,[1] and Douglas A. Bell[1,4,*]

[1]Environmental Epigenomics and Disease Group, Immunity, Inflammation, and Disease Laboratory, National Institute of Environmental Health Sciences, National Institutes of Health, Research Triangle Park, NC 27709, USA

[2]Integrative Bioinformatics Support Group, National Institute of Environmental Health Sciences, National Institutes of Health, Research Triangle Park, NC 27709, USA

[3]These authors contributed equally

[4]Lead Contact

*Correspondence: bell1@niehs.nih.gov

https://doi.org/10.1016/j.xcrm.2020.100054

SUMMARY

Tobacco smoke exposure contributes to the global burden of communicable and chronic diseases. To identify the immune cells affected by smoking, we use single-cell RNA sequencing on peripheral blood from smokers and nonsmokers. Transcriptomes reveal a subpopulation of *FCGR3A* (CD16)-expressing natural killer (NK)-like CD8 T lymphocytes that increase in smokers. Mass cytometry confirms elevated CD16$^+$ CD8 T cells in smokers. Inferred as highly differentiated by pseudotime analysis, NK-like CD8 T cells express markers that are characteristic of effector memory re-expressing CD45RA T (T_{EMRA}) cells. Indicative of immune aging, smokers' CD8 T cells are biased toward differentiated cells, and smokers have fewer naive cells than nonsmokers. DNA methylation-based models show that smoking dose is associated with accelerated aging and decreased telomere length, a biomarker of T cell senescence. Immune aging accompanies T cell senescence, which can ultimately lead to impaired immune function. This suggests a role for smoking-induced, senescence-associated immune dysregulation in smoking-mediated pathologies.

INTRODUCTION

As a risk factor for human diseases, the global disease burden attributed to tobacco smoke exposure is substantial. The World Health Organization (WHO) estimates ~6 million deaths per year from tobacco smoke exposure, resulting from both chronic and communicable diseases.[1,2] In smokers, a decline in immunity and an increased risk of inflammatory diseases, such as atherosclerosis, make the argument that smoking-associated diseases are mediated by immune dysfunction. The development and progression of atherosclerotic lesions serves as an example of a complex immune-mediated pathology because T cells, monocytes, macrophages, dendritic cells (DCs), and B cells have been reported to be involved.[3,4] Refining smoking-associated changes within immune populations will enhance our understanding of how dysfunctional immune subsets arise from exposure to tobacco smoke. This will facilitate the prevention of diseases by identifying immune cells to target for clinical intervention.

Smoking alters the epigenome and transcriptome of human blood leukocytes, in addition to DNA damage.[5-7] In the article by Su et al.,[5] we demonstrated that changes identified in isolated cell fractions, which correspond to major immune populations, were distinct from one another and whole blood. For example, *ITGAL*, expressed in T cells and involved in inflammation,[8] had decreased methylation in smokers' T cells but not in whole blood or isolated cell fractions. It follows that bulk data from isolated fractions, comprising multiple subtypes, would similarly mask meaningful changes, especially when differences arise in low-frequency subsets. As such, the interpretation of bulk genomic approaches is limited because changes could indicate an altered distribution of cell (sub)populations or changes in expression within (sub)populations. The recent development of single-cell methods provides the technology to resolve smoking-associated (sub)population composition changes, examine gene expression differences, and identify rare subtypes obscured by bulk fraction data. In addition, multiparameter data allow us to concordantly study multiple cell types from the same individuals.

To identify smoking-affected cell (sub)populations and connect observed immune cell changes with smoking-associated diseases, we characterized gene expression profiles and cell surface marker phenotypes from primary peripheral blood mononuclear cells (PBMCs) from four nonsmokers and four smokers by single-cell RNA sequencing (scRNA-seq) and mass cytometry. The combination of transcriptome profiling and immunophenotyping provides higher confidence in the validity of our findings than one single-cell method alone. Major population frequencies showed a strong correlation between scRNA-seq and mass cytometry. We used single-cell transcriptome profiling to further separate cell populations into multiple

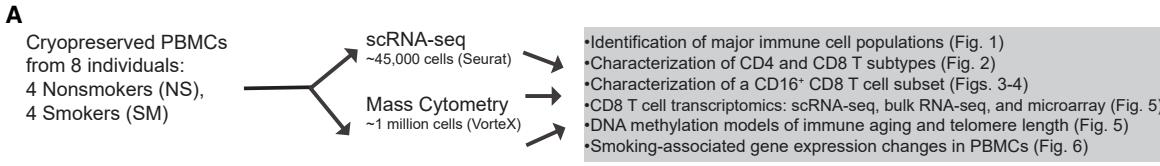

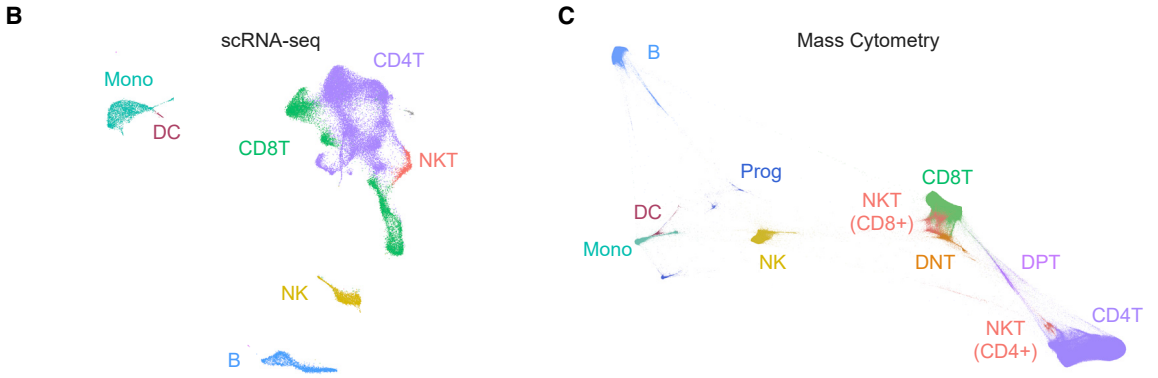

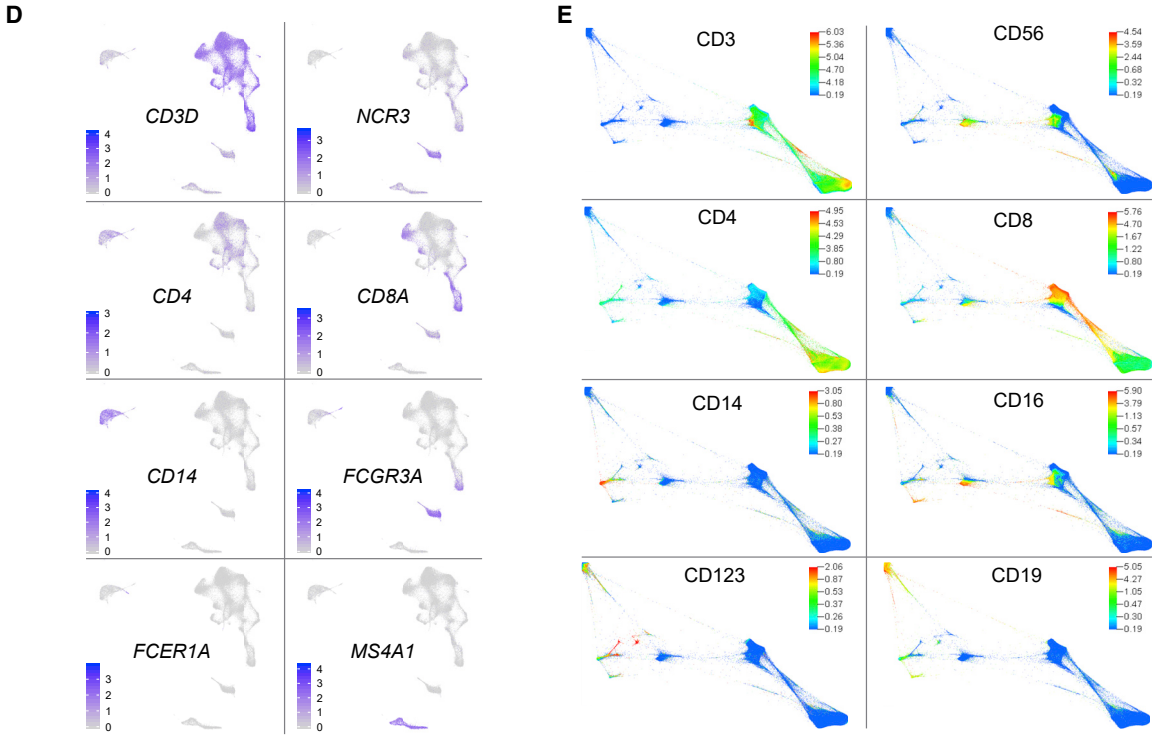

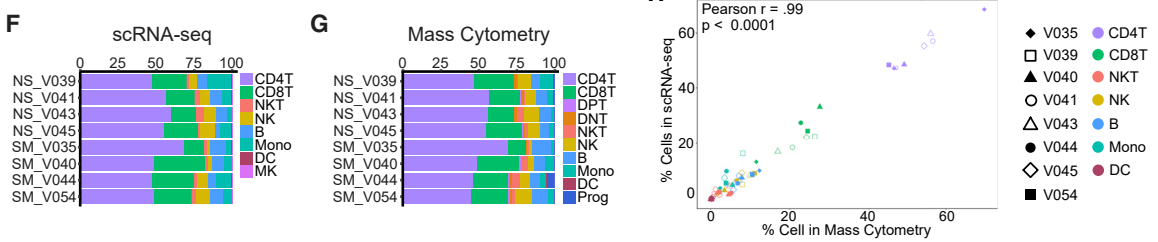

(legend on next page)

subsets according to differentiation, activation, or functional states. We found a population of $CD16^+$ CD8 T cells that was increased in smokers and exhibited natural killer (NK)-like transcriptional programs. Pseudotime analysis and examination of canonical markers revealed that these NK-like CD8 T cells likely represent a terminally differentiated state. DNA methylation models demonstrated that the smoking dose was associated with accelerated immune aging and decreased telomere length (TL; a biomarker of T cell senescence) in CD8 T cells. Not limited to CD8 T cells, smokers' other immune populations displayed senescent characteristics.

By detecting an altered abundance of a rare population, we revealed an immune target that can be isolated and explored for connections between smoking and chronic diseases. Combined with increased (pre-)senescent CD8 T cells, elevated regulatory T cells (Tregs) and induction of senescence-linked genes in multiple cell types provide evidence that smokers show signs of premature immune system aging. The potential immune function defects and inflammatory subsets demonstrated here mirror the characteristics of pathologies commonly found in smokers. Further studies of smoking-associated dysregulation of immune transcriptional programs and candidate dysfunctional T cells linked to accelerated immune system aging will lead to mechanistic insights to advance disease prevention strategies for smoking-mediated pathologies.

RESULTS

scRNA-Seq and Mass Cytometry Profiling of Human Peripheral Blood Immune Cells in Smokers and Nonsmokers

We set out to characterize the effects of cigarette smoke on immune cells in peripheral blood using single-cell approaches to determine whether the smoking-associated gene expression changes observed within major immune cell populations resulted from an altered abundance of specific, identifiable cell subsets. We performed scRNA-seq and mass cytometry in parallel on cryopreserved peripheral blood samples from eight donors with no history of atherosclerosis, chronic obstructive pulmonary disease (COPD), or lung cancer (Figure 1A). Serum cotinine, a metabolite of nicotine and an established biomarker of recent cigarette smoke exposure,[9] confirmed the smoking status of donors. Smokers (n = 4) used for single-cell analyses had serum cotinine levels ranging from 240 to 511 ng/mL; all nonsmokers (n = 4) had serum cotinine levels <2 ng/mL. Donors were matched based on gender and race; ages ranged from 31 to 56 years and were not significantly different between smokers and nonsmokers (p = 0.23). Demographic and smoking information is listed in Table S1. We obtained single-cell mRNA data from 45,049 cells and surface protein expression data from 990,748 cells.

For each single-cell approach, we assigned cells to common immune populations based on mRNA (scRNA-seq) or surface protein (mass cytometry) expression (Figures 1B–1E; Table S2). For scRNA-seq, we used Seurat[10,11] to integrate data and implement shared nearest neighbors (SNN) clustering (see STAR Methods). We then used Model-based Analysis of Single-cell Transcriptomics (MAST[12]) to identify positive and negative marker genes for each cluster and combined cells into major immune populations (Table S2). Cells in clusters expressing *CD3D* as a positive marker were designated as T cells (Figure 1D). T cells were further classified into CD4 T cells, CD8 T cells, or NKT cells based on the expression of *CD4*, *CD8A*, or *NCR3* (Figure 1D). NK cells were identified based on *CD3D* as a negative marker combined with the expression of *NKG7*, *GNLY*, *GZMB*, *PRF1*, and *NCR3* as positive markers (Figure 1D; Table S2). Monocytes were positive for *LYZ* and either *CD14* or *FCGR3A* (encodes CD16), characteristic of classical or nonclassical monocytes (Figure 1D). DCs were similar to monocytes but could be distinguished by the expression of *FCER1A* (Figure 1D). B cells were defined by *MS4A1* (encodes CD20; Figure 1D).

In parallel, PBMCs from each donor were assessed by mass cytometry (see STAR Methods). Viable, single-cell events were manually gated using Cytobank[13] (Figure S1A). We used VorteX[14] to cluster and create a force-directed layout (FDL) graph using the X-shift algorithm (see STAR Methods). A total of 122 PBMC cell clusters were determined from the 8 donors representing 983,848 cells (Figure S1B) and shown by smoking status (Figure S1C). Cell surface protein expression profiles were used to classify the cell populations (Figures 1C and 1E). T cells displayed CD3 and were classified by CD4 and CD8 as double-negative (DNT), double-positive (DPT), CD4 T, or CD8 T cells (Figures 1C and 1E). NKT cells were identified by CD3 and CD56 with CD4 or CD8 protein expression markers. Monocytes expressed CD14 and/or CD16 and DCs had CD123 above background levels (Figure 1E). B cells were positive for CD19 (Figure 1E). NK cells were positive for CD56 but negative for CD3 (Figure 1E).

To determine how well the scRNA-seq and mass cytometry corresponded with each other, we examined the individual donor proportion for each cell type. Cells colored by individual donors are shown for scRNA-seq (Figure S1D) and mass

Figure 1. scRNA-Seq and Mass Cytometry Profiling of Human PBMCs from Smokers (n = 4) and Nonsmokers (n = 4)

(A) Experimental design: cryopreserved PBMCs from smokers and nonsmokers were thawed for scRNA-seq and mass cytometry.

(B) Uniform Manifold Approximation and Projection (UMAP) scRNA-seq plot: ~45,000 PBMCs colored by major cell type.

(C) Force directed layout (FDL) of mass cytometry: ~1 million cells colored by major cell type.

(D) Canonical gene expression markers for major cell types: CD8T cells (*CD3D*, *CD8A*), CD4T cells (*CD3D*, *CD4*) natural killer T (NKT) cells (*CD3D*, *NCR3*), natural killer (NK) cells (*NCR3*), monocytes (*CD14*, *FCGR3A* [CD16]), dendritic cells (DCs; *FCER1A*), and B cells (*MS4A1*).

(E) Cell surface protein expression for major cell types: CD8T cells (CD3, CD8a), CD4T cells (CD3, CD4), NKT cells (CD3, CD56), NK cells (CD56), monocytes (CD14, CD16), DCs (CD123) and B cells (CD19).

(F and G) Major cell type frequency distributions by individual donor (nonsmokers, NS; smokers, SM) colored by cell type for scRNA-seq (F) and mass cytometry (G).

(H) Major cell type frequencies showed strong correlation between scRNA-seq and mass cytometry (Pearson r = 0.99, r^2 = 0.98, p < 0.0001). Shapes represent matched individuals, NS (unfilled) and SM (filled), are colored by cell type.

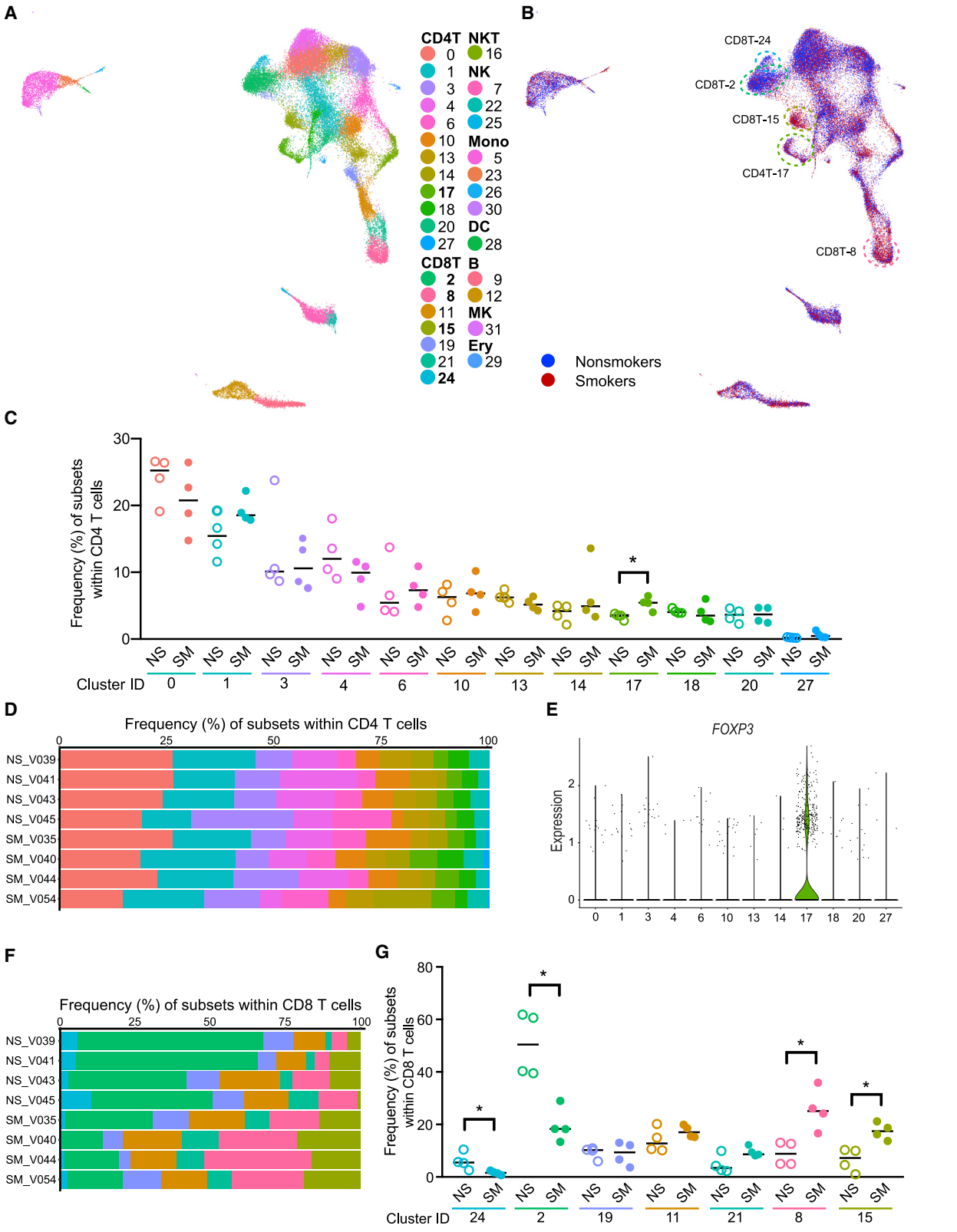

(legend on next page)

cytometry (Figure S1E). Cell-type frequencies were calculated and plotted to compare frequency distributions among individuals (Figures 1F and 1G). For both methods, all of the major populations—CD4T, CD8T, NKT, B, monocyte, and DC—were identified in all of the donors. We then compared the frequency of major populations in PBMCs by smoking status for scRNA-seq and mass cytometry using a Mann-Whitney *U* test. We observed no differences in the overall frequency of major cell types between smokers and nonsmokers by either scRNA-seq or mass cytometry (Figures S1F and S1G). Comparison of the major immune population percentages among individuals for scRNA-seq and mass cytometry showed significant strong correlation (Pearson r = 0.99, r^2 = 0.98, $p < 0.0001$) between methods (Figure 1H).

scRNA-seq Reveals Increased Tregs and Altered Composition of the CD8 T Cell Population between Smokers and Nonsmokers

Single-cell transcriptome profiling can be used to separate cell populations into multiple subsets according to differentiation, activation, or functional states. Based on gene expression patterns, we clustered peripheral blood cells into 31 immune cell clusters and 1 erythroid contaminant cluster, labeled based on abundance from 0 (most abundant) through 31 (Figure 2A; Table S2). We identified 12 CD4 T cell (0, 1, 3, 4, 6, 10, 13, 14, 17, 18, 20, and 27), 7 CD8 T cell (2, 8, 11, 15, 19, 21, and 24), 3 NK cell (7, 22, and 25), 4 monocyte (5, 23, 26, and 30), and 2 B cell (9 and 12) clusters. NKTs (16), DCs (28), and MKs (31) were each contained by a single cluster. Here, clusters are referred to by major immune cell type, followed by original cluster identification (ID) (e.g., CD4T-0). To determine whether smoking altered the subtype distributions within the major cell populations, we compared the abundance of cells among clusters for each major cell type that separated into more than one cluster. Cells colored by smoking status are shown in Figure 2B. We did not observe any subset frequency shifts in B cells, monocytes, or NK cells (Figures S2A–S2F).

For 11 of 12 CD4 T cell subsets, frequencies were not significantly altered by smoking (Figures 2B and 2C). Although donors exhibited interindividual variation, smoking status did not appear to have a considerable impact on the distribution of CD4 T cells (Figure 2D). Only one cluster, CD4T-17, was higher in smokers than in nonsmokers ($p < 0.05$; Figure 2C). This cluster was relatively low in abundance among CD4 T cell subsets: a median 3.5% in nonsmokers and 5.4% in smokers. We characterized CD4T-17 cells as Tregs based on elevated *FOXP3* and *IL2RA* (encodes CD25; Figure 2E; Table S2). No other CD4T clusters showed *FOXP3* or *IL2RA* as strong positive markers. DNA methylation level of the *AHRR* gene can be used as a dose- and duration-dependent biomarker of tobacco smoke exposure; *AHRR* methylation is strongly negatively correlated with smoking dose and duration.[6,15,16] The elevated frequency of Tregs was associated with reduced *AHRR* DNA methylation in whole blood ($p = 0.002$, $r^2 = 0.81$; Figure S2G).

In contrast to most CD4 T cell subsets, the variation among donors in CD8 T cells depended on smoking status, as illustrated by the differences in the dominant population(s) in CD8 T cells from smokers and nonsmokers (Figure 2F). Smokers had lower proportions of 2 CD8 T cell clusters (CD8T-24 and CD8T-2) and higher proportions of 2 CD8 T cell clusters (CD8T-8 and CD8T-15) compared to nonsmokers ($p < 0.05$; Figure 2G). We did not observe significant differences in the proportions of the remaining 3 CD8 T cell clusters (CD8T-19, CD8T-11, and CD8T-21).

CD8 T Cell Distribution Shifts from Naive to Differentiated States in Smokers

Smoking had substantial effects on the composition of CD8 T cells. We further analyzed each of the seven CD8 T clusters to identify distinct gene expression patterns. MAST identified positive and negative markers for each CD8 T cluster relative to other CD8 T cells (see STAR Methods). We found 71, 223, 46, 144, 71, 739, and 105 positive and 86, 978, 10, 68, 59, 214, and 52 negative markers (Bonferroni adjusted $p < 0.05$ in both smokers' and nonsmokers' cells) for CD8T-24, CD8T-2, CD8T-19, CD8T-11, CD8T-21, CD8T-8, and CD8T-15 clusters, respectively (Table S3). We examined marker lists for genes associated with T cell differentiation and function to distinguish between CD8 T subsets. Genes frequently used to classify CD8 T subsets varied among CD8 T cell clusters (Figures 3A and 3B). Elevated *CCR7*, *SELL*, and *IL7R* combined with low *CCL5* indicated that clusters CD8T-24 and CD8T-2 represented naive cells (T_N). High levels of *IL7R*, *SELL*, and *FOS* (activated T cell proliferation[18,19]) suggested that cluster CD8T-15 exhibited characteristics of long-lived memory cells, such as central memory T cells (T_{CM}). Reduced levels of *CCR7*, *SELL*, and *IL7R* and elevated *CCL5* and *KLRG1* in CD8T-11, CD8T-21, and CD8T-8 are indicative of later differentiation stages (e.g., T_{EM}). The lack of *CD27* expression and decrease in *FOS* in CD8T-21 and CD8T-8 indicated highly differentiated T_{EM} cells (i.e., T_{EMRA}). *ZEB2*, associated with terminal differentiation states,[20,21] was detected in approximately one-third of CD8T-8 cells (35.1% in smokers and 28.2% in nonsmokers).

Several clusters exhibited intermediate expression of differentiation state genes. To organize CD8 T cell clusters by their likely differentiation trajectories, we used the Slingshot algorithm[22] to

Figure 2. Increased CD4 Tregs and Altered CD8 T Cell Composition Observed between Smokers (SM, n = 4) and Nonsmokers (NS, n = 4)

(A) scRNA-seq UMAP colored by cluster ID.

(B) scRNA-seq UMAP colored by smoking status. Clusters CD8T-24 and CD8T-2 had more cells from nonsmokers and CD4T-17, CD8T-15, and CD8T-8 had more cells from smokers.

(C and D) Subset frequencies within CD4 T cells. Smokers (filled) had a significant increase in cluster CD4T-17 compared to nonsmokers (unfilled). Bar = median, *$p < 0.05$ by Mann-Whitney *U* test (C). Individual donor distribution of CD4 T cell subsets (D).

(E) *FOXP3* gene expression within CD4 T subsets.

(F and G) Subset frequencies within CD8 T cells. Individual donor distribution of CD8 T cell subsets (F). Smokers (filled) had significant decreases in clusters CD8T-24 and CD8T-2 and increases in clusters CD8T-8 and CD8T-15 compared to nonsmokers (unfilled). Bar = median, *$p < 0.05$ by Mann-Whitney *U* test (G).

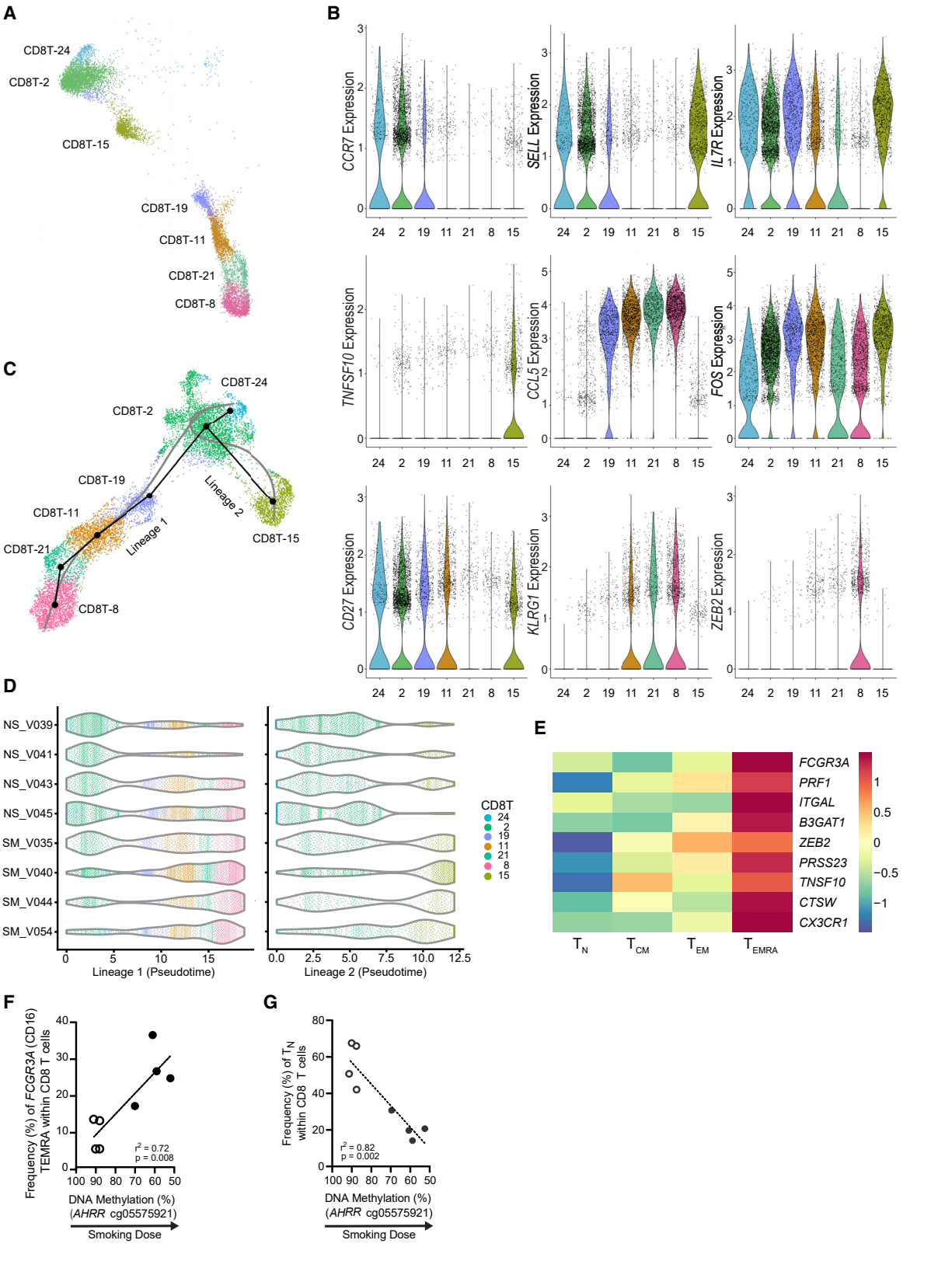

(legend on next page)

perform pseudotemporal analysis. Lineage inference ordered CD8 T cells into 2 lineages, which originate from cluster CD8T-24 and terminate at either cluster CD8T-8 or CD8T-15 (Figure 3C). Lineage 1 mostly comprised cells from CD8T-24, CD8T-2, CD8T-19, CD8T-8, CD8T-21, and CD8T-8, with minimal cells from CD8T-15. Lineage 2 mostly comprised cells from CD8T-24, CD8T-2, and CD8T-15, with minimal cells from CD8T-19. Based on the altered composition of CD8 T cell subsets—lower proportions of CD8T-2 and CD8T-24 and higher proportions of CD8T-8 and CD8T-15 cells (Figures 2B, 2F, and 2G)—we propose that tobacco smoke exposure alters CD8 T cell composition by shifting CD8 T cells toward differentiated states. Smokers' cells were biased toward later pseudotimes in both lineages (Figure 3D), demonstrating that smokers' CD8 T cells are skewed toward differentiated states and nonsmokers' CD8 T cells are skewed toward naive states.

We next identified temporally associated genes for each lineage. Only 10 genes within the top 100 temporally expressed genes were shared, and most shared genes exhibited the same direction of change over pseudotime in both lineages (Figures S3A and S3B). In general, temporally expressed genes for CD8 T cell lineages were consistent with effector memory (lineage 1) and central memory (lineage 2) differentiation. For example, in lineage 1, *CCL5* and *NKG7* increased, while *SELL* and *IL7R* decreased over the differentiation trajectory (Figures S3A and S3C). *CMC1* demonstrated a nonlinear association in lineage 1, as it peaked in CD8T-21 cells and then decreased through CD8T-8 cells (Figures S3A and S3C).

The terminal cluster in the effector memory trajectory, CD8T-8, shared many features with the penultimate cluster, CD8T-21; however, CD8T-8 increased in smokers, but CD8T-21 did not. Since the low expression of *CD27* and *CCR7* and elevated expression of *KLRG1* in both clusters would classify these cells as highly differentiated CD8 T cells (i.e., T_{EMRA}-like), we sought to find markers within CD8T-8 that did not occur in CD8T-21. Examination of exhaustion markers—*TOX*, *PDCD1* (encodes programmed cell death protein-1 [PD-1]), *CTLA4*, and *HAVCR2* (encodes TIM3)—did not distinguish the clusters. Whereas smokers' CD8T-8 cells had elevated expression of *TOX* (log_2FC [fold change] = 0.31, p = 1.44×10^{-9}), nonsmokers' CD8T-8 cells did not, and no other exhaustion markers were significantly elevated (Table S3). We next examined senescence-associated genes *KLRG1* and *B3GAT1* (encodes CD57). While *KRLG1* was a positive marker for CD8T-21 (smokers [SM]: $log_2FC = 0.65$, $p = 8.11 \times 10^{-04}$; nonsmokers [NS]: $log_2FC = 1.33$, $p = 2.23 \times 10^{-22}$) and CD8T-8 cells (SM: $log_2FC = 0.94$, $p = 6.29 \times 10^{-47}$; NS: $log_2FC = 1.28$, $p = 1.94 \times 10^{-40}$), *B3GAT1* was unique to CD8T-8 cells (SM: $log_2FC = 0.19$, $p = 3.83 \times 10^{-14}$; NS: $log_2FC = 0.10$, p = 0.022). We also found that 2 genes reported as having smoking-associated methylation changes, *GFI1* and *PRSS23*,[15] showed elevated expression in CD8T-8 cells (*GFI1* SM: $log_2FC = 0.20$, $p = 5.58 \times 10^{-7}$; *GFI1* NS: $log_2FC = 0.22$, p = 0.046; *PRSS23* SM: $log_2FC = 1.07$, $p = 1.5 \times 10^{-143}$; *PRSS23* NS: $log_2FC = 0.91$, $p = 7.7 \times 10^{-60}$). *FCGR3A*, commonly found on NK cells and nonclassical monocytes, was identified as a strong positive marker of CD8T-8 cells in smokers ($log_2FC = 1.63$, $p = 1.17 \times 10^{-171}$) and nonsmokers ($log_2FC = 1.72$, $p = 5.17 \times 10^{-119}$; Figure 1D; Table S3).

We reanalyzed the gene expression data from flow-sorted human peripheral naive ($CD27^+CD45RA^+$), central memory ($CD27^+CD45RA^-$), effector memory ($CD27^-CD45RA^-$), and EMRA ($CD27^-CD45RA^+$) CD8 T cells from healthy adults.[17] We found that the T_{EMRA} subset had an increased expression of *FCGR3A* (Figure 3E). Combined with our finding of high *FCGR3A* in our most differentiated CD8 T cluster (CD8T-8), data from Callender et al.[17] supports elevated *FCGR3A* as a characteristic of CD8 T_{EMRA} cells. In addition, CD8 T_{EMRA} cells showed an elevated expression of senescence-associated secretory phenotype (SASP) genes (Figure 3E).

Given that human cytomegalovirus (HCMV) infection can alter T cell composition,[23,24] we tested donors for HCMV antibodies and DNA in serum (see STAR Methods). Compared to seronegative donors (immunoglobulin G $[IgG]^-/IgM^-$), seropositive donors (IgG^+/IgM^-) had elevated levels of CD8 T_{EMRA} cells (CD8T-21), but not *FCGR3A*-expressing CD8 T_{EMRA} cells (CD8T-8); neither naive CD8 T clusters (CD8T-24 and CD8T-2) were significantly reduced in HCMV seropositive donors (Figure S3D; Table S1).

To further support the idea that smoking elevated *FCGR3A*-expressing CD8 T_{EMRA} cells (CD8T-8) and reduced naive CD8 T cells (CD8T-24 and CD8T-2), we compared the frequencies of these subpopulations against whole-blood DNA methylation of *AHRR* (Figures 3F and 3G; Table S1). A higher frequency of *FCGR3A*-expressing CD8 T_{EMRA} cells was associated with reduced *AHRR* methylation (p = 0.008, $r^2 = 0.72$), and a lower frequency of naive CD8 T cells was associated with reduced *AHRR* methylation (p = 0.002, $r^2 = 0.82$). In addition, the increase in *FCGR3A*-expressing CD8 T_{EMRA} cells was highly correlated with the increase in CD4 Tregs (p = 0.019, $r^2 = 0.63$; Figure S3E).

Mass Cytometry Confirms Elevated $CD16^+$ CD8 T Cells in Smokers

Relatively rare in nonsmokers (median: 1.8%), the *FCGR3A*-expressing CD8 T cell cluster (CD8T-8) comprised 7.3% of PBMCs

Figure 3. CD8 T Cell Subsets Shift from Naive to Differentiated CD8 T Cell States

(A) scRNA-seq UMAP (n = 8) of the 7 CD8 T cell subsets colored by cluster ID.

(B) Expression of genes to characterize CD8 T subsets. Color indicates cluster ID (n = 8).

(C) Trajectory inference (pseudotime analysis) ordered CD8 T cell clusters into 2 lineages, which originate from cluster CD8T-24 and terminate at either cluster CD8T-8 (lineage 1) or CD8T-15 (lineage 2). The black line shows lineages and the gray line shows simultaneous principle curves (n = 8).

(D) Pseudotime for CD8 T cells by individual nonsmokers (NS, n = 4) and smokers (SM, n = 4) in lineage 1 (left) and lineage 2 (right).

(E) Gene expression data[17] from flow-sorted human peripheral CD8 T cells (n = 6): naive (T_N; $CD27^+CD45RA^+$), central memory (T_{CM}; $CD27^+CD45RA^-$) effector memory (T_{EM}; $CD27^-CD45RA^-$), and EMRA (T_{EMRA}; $CD27^-CD45RA^+$). *FCGR3A* (false discovery rate [FDR] = 1.38×10^{-8}), *PRF1* (FDR = 2.69×10^{-6}), and *ITGAL* (FDR = 5.43×10^{-3}), are positive markers for CD8T-8 cells; *B3GAT1* (CD57; FDR = 1.06×10^{-5}) and *ZEB2* (FDR = 2.16×10^{-5}) are positive markers for CD8T-8 cells and indicators of senescence; *PRSS23* (FDR = 8.62×10^{-4}), *TNFSF10* (FDR = 6.46×10^{-3}), and *CTSW* (FDR = 2.52×10^{-3}) are secreted factors associated with SASP; and *CX3CR1* (FDR = 8.95×10^{-6}) is a chemokine receptor.

(F and G) Frequency of *FCGR3A* CD8 T_{EMRA} (F) and CD8 T_N (G) cells are correlated with smoking dose as measured by *AHRR* smoking biomarker (n = 8).

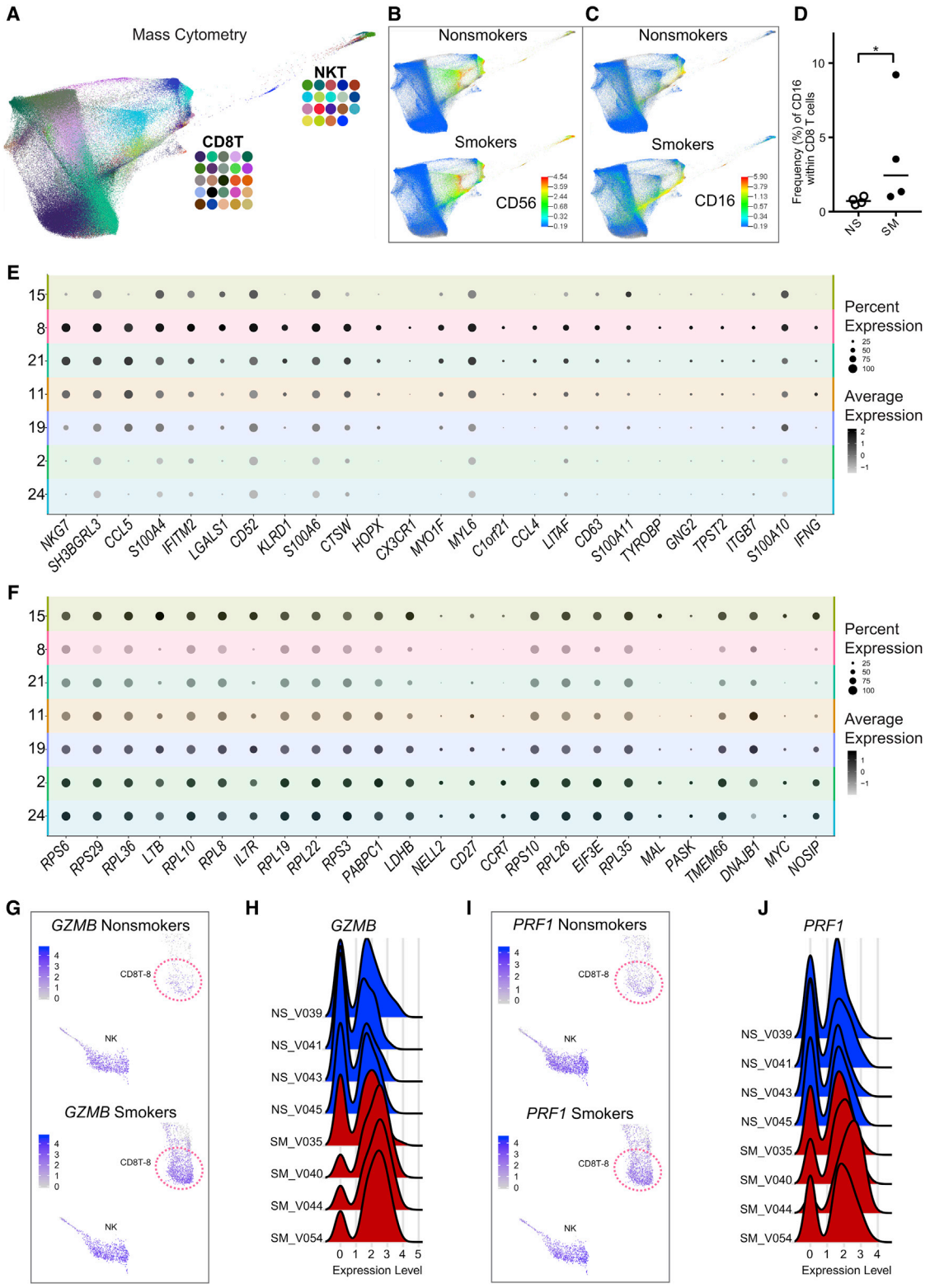

Figure 4. Characterization of CD16⁺ CD8 T Cells

(A–D) Mass cytometry confirms elevated proportion of CD16⁺ CD8 T cells in smokers.

(A) FDL (n = 8) of CD8 T and NKT cells colored by cluster ID.

(B and C) Cell surface marker intensity for NK marker CD56 (B) and CD16 (C) in nonsmokers (top, n = 4) and smokers (bottom, n = 4).

(legend continued on next page)

in smokers. Reported as a low-frequency subset (~2% of PBMCs in healthy adults), $CD16^+$ CD8 T cells have been described.[25-27] Based on these reports, we sought to ascertain whether smokers had increased levels of $CD16^+$ CD8 T cells that expressed surface proteins for CD3, but not CD56; i.e., confirm an increase in CD16 expression within CD8 T cells that are not NKT cells. To show that smokers had increased surface protein expression of CD16 within their CD8 T cells, we ran X-shift on all CD8 T and NKT cells and visualized the FDL colored by cluster IDs (Figure 4A). We did not see any differences between smokers' and nonsmokers' CD8 T cells for CD56 (Figure 4B), but smokers showed an increase in the proportion of CD8 T cells expressing CD16 compared to nonsmokers (Figure 4C). We determined the frequency of $CD16^+$ CD8 T cells in smokers and nonsmokers by manual gating (Figure S4A). $CD3^+CD56^-$ negative cells were then gated to obtain single positive CD8 T cells ($CD3^+CD56^-CD8^+CD4^-$; Figure S4A), which were then used to determine the frequency of $CD16^+$ CD8 T cells ($CD3^+CD56^-CD8^+CD4^-CD16^+$; Figure S4A). Compared to nonsmokers, smokers had a significantly increased frequency of $CD16^+$ CD8 T cells ($p = 0.03$; Figure 4D), confirming that smokers had elevated proportions of $CD16^+$ CD8 T cells. In an independent group of donors, $CD16^+$ CD8 T cells were also elevated in smokers compared to nonsmokers ($p < 0.01$; Figure S4B; Table S1).

To phenotype the $CD16^+$ CD8 T cell subset, we gated $CD3^+$ T cells by a CD45RA/CD45 biaxial plot to establish an accurate $CD45RA^+$ gate that was then applied to the $CD16^+$ CD8 T cells (Figure S4C). Consistent with a T_{EMRA} phenotype, the majority of $CD16^+$ CD8 T cells were positive for CD45RA in both smokers and nonsmokers (Figure S4D).

FCGR3A-Expressing CD8 T Cells Exhibit NK-like Transcriptome Signatures

After confirming an increase in $CD16^+$ CD8 T cells in smokers, we further examined how the transcriptomes of *FCGR3A*-expressing CD8 T cells differed from other CD8 T cells. In addition to *FCGR3A*, CD8T-8 cells exhibited elevated expression *NKG7*, *GNLY*, *FGFBP2*, *GZMB*, and *PRF1* (Tables S2 and S3). While these genes are considered cytotoxic T or NK cell-expression signatures, the presence of CD16 led us to suspect that this subset may express genes indicative of NK-like attributes. To gain insight into the functional relevance of gene expression profiles for CD8T-8 cells, we performed gene set enrichment analysis (GSEA). Consistent with an NK-like transcriptional program, "LI INDUCED T TO NATURAL KILLER UP" had a positive normalized enrichment score (NES = 1.88, FWER < 0.05) and "GSE22886 NAIVE TCELL VS NKCELL UP" had a negative NES (−2.13, FWER < 0.05). The "LI INDUCED T TO NATURAL KILLER UP" gene set encompasses expression patterns for T cells reprogrammed to have NK-like phenotypes—"induced T to NK" (iTNK) cells.[28] Here, we found 67 and 71 genes from the iTNK gene signature as positive markers ($p < 0.05$) of *FCGR3A*-expressing CD8 T cells in smokers and nonsmokers, respectively. Figure 4E shows the 25 highest ranked iTNK genes, based on p value in CD8T-8 cells. CDT8-8 genes were negatively enriched (FWER < 0.05) for genes that are higher in naive CD8 T cells relative to NK cells ("GSE22886 NAIVE TCELL VS NKCELL UP"). Smokers' and nonsmokers' CD8T-8 cells had significantly reduced expression (i.e., negative markers) of 55 and 45 naive CD8 T versus NK genes. Figure 4F shows the 25 highest ranked naive CD8 T versus NK genes, based on p value for CD8T-8 cells.

To examine whether smokers' "NK-like" CD8 T cells differed from those of nonsmokers, we compared the average expression of genes from smokers' CD8T-8 cells to nonsmokers' CD8T-8 cells (see STAR Methods). We found that 63 genes had an increased and 74 genes had a decreased average per cell expression in smokers compared to nonsmokers ($p < 0.05$; Table S4). Figures S4E and S4F show 25 genes with increased and decreased per cell expression, ordered by the difference in the percentage of cells expressing each gene between smokers and nonsmokers. Although cellular mRNA levels for effector molecules granzyme B (encoded by *GZMB*) and perforin (encoded by *PRF1*) exhibited interindividual variation, both increased in frequency of expression and average per-cell expression in smokers compared to nonsmokers (Figures 4G–4J, S4E, S4G, and S4H).

CD8 T Bulk Transcriptomes Reflect Differentiation State Shifts Observed at the Single-Cell Level

To assess the overall impact of smoking on CD8 T cells, we identified differentially expressed genes (DEGs) between smokers and nonsmokers by comparing the average per-cell expression for all of the cells in the 7 CD8 T clusters combined. Of 2,163 genes evaluated in the pseudobulk analysis, we found that 1,817 genes had higher expression and 344 genes had lower expression in smokers versus nonsmokers ($q < 0.05$; Table S5). To examine the interindividual variability in response to smoking, we performed hierarchical clustering using smoking scRNA-DEGs, which separated individual donors by smoking status (Figures 5A and S5A). To validate altered CD8 T gene expression profiles in smokers, we used RNA-seq and microarray on isolated CD8 T cells to examine the differences in bulk RNA expression.

(D) Frequency of $CD16^+$ cells increases within CD8 T cells in smokers (filled, n = 4) compared to nonsmokers (unfilled, n = 4). Bar = median, *$p < 0.05$ by 1-tailed Mann-Whitney *U* test.

(E and F) NK-associated transcriptome characteristics (n = 8) revealed in CD8T-8 cells by gene set enrichment analysis (GSEA). CD8T-8 cells were positively enriched (FWER < 0.05) for gene signatures of T cells induced to have NK-like phenotypes; split dot plot shows 25 genes within the induced T to NK gene set (E). CD8T-8 cells were negatively enriched (FWER < 0.05) for genes higher in naive CD8 T cells relative to NK cells; split dot plot shows 25 genes within the naive T versus NK gene set (F). Color intensity represents average per-cell expression (scale shows standard deviation), and circle size indicates the percentage of cells expressing each gene.

(G and H) CD8T-8 cells show increased *GZMB* expression in smokers. (G) UMAP comparison of *GZMB* between nonsmokers' (top, n = 4) and smokers' (bottom, n = 4) cells. Cluster CD8T-8 is indicated by dotted circle. (H) Individual donor *GZMB* levels for CD8T-8 cells for nonsmokers (NS, n = 4) and smokers (SM, n = 4).

(I and J) CD8T-8 cells have increased *PRF1* expression in smokers. (I) UMAP comparison of *PRF1* between nonsmokers' (top, n = 4) and smokers' (bottom, n = 4) cells. Cluster CD8T-8 is indicated by dotted circle. (J) Individual donor *PRF1* levels for CD8T-8 cells for nonsmokers (NS, n = 4) and smokers (SM, n = 4).

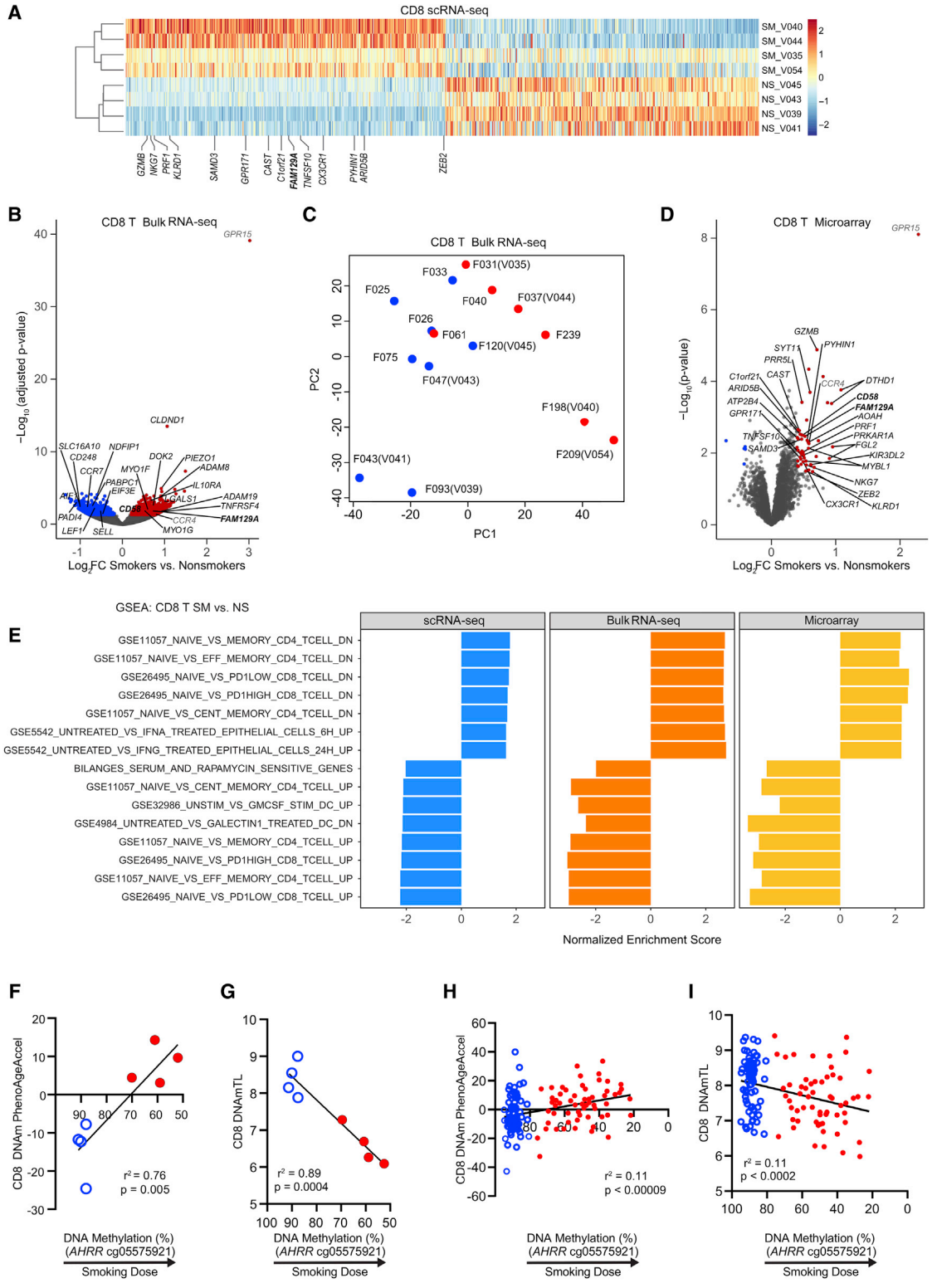

(legend on next page)

Isolated CD8 T cells for bulk RNA-seq included the 8 donors used in scRNA-seq (bulk RNA was from a previous visit) and 7 additional donors (Table S1). We identified 1,268 genes as differentially expressed—692 increased and 576 decreased ($q < 0.05$; Figure 5B). With the exception of F061, principal-component analysis (PCA) of bulk RNA-seq data separated smokers from nonsmokers (Figure 5C). We evaluated microarray data from isolated CD8 T cells from 19 donors (9 smokers and 10 nonsmokers). Isolated CD8T cells included 4 donors used in scRNA-seq, 4 donors used in bulk RNA-seq, and 11 additional donors (Table S1). We identified 51 DEGs (see STAR Methods)—46 increased and 5 decreased (Figure 5D).

We compared results from the 3 RNA analysis platforms used to identify smoking-associated DEGs in CD8 T cells. Bulk RNA-seq confirmed 241 smoking DEGs from the scRNA-seq, 162 with increased and 79 with decreased expression in smokers compared to nonsmokers (Figures 5B; Table S5). Microarray analysis confirmed 24 smoking DEGs that were identified by scRNA-seq as increased in smokers compared to nonsmokers (Figures 5A and 5D; Table S5). Two genes, *FAM129A* and *CD58*, increased in smokers' CD8 T cells in all 3 platforms (Figures 5A, 5B, 5D, S5A, and S5B; Table S5). Genes found to be altered by at least 2 methods include *LGALS1*, *ADAM8*, and *CLDND1*, which were increased in bulk RNA-seq and scRNA-seq data; *GPR15*, which was increased in the bulk RNA-seq and microarray data; and *NDFIP1*, which was decreased in the bulk RNA-seq and scRNA-seq data (Figures 5A, 5B, 5D, and S5A–S5F). *ITGAL*, a smoking methylation biomarker,[5] was only found to be significantly increased by scRNA-seq ($\log_2FC = 0.36$, $p = 1.70 \times 10^{-26}$), and was also elevated in the NK-like subset (SM: $\log_2FC = 0.64$, $p = 6.53 \times 10^{-29}$; NS: $\log_2FC = 0.78$, $p = 1.50 \times 10^{-20}$).

Although each platform identified smoking DEGs not found by other platforms, we expect the overall changes observed to represent a similar shift in the functional states of CD8 T cells. We used GSEA to determine that CD8 T pseudobulk and bulk transcriptomes were enriched for similar functional annotations. Pseudobulk scRNA-seq, bulk RNA-seq, and bulk microarray shared 7 positively and 8 negatively enriched gene sets (FWER < 0.05; Figure 5E). CD8 T cells were positively enriched for genes with a higher expression in memory T, T_{CM}, T_{EM}, $PD1^{lo}$ (CD8 T_{EM}), and $PD1^{hi}$ (CD8 T_{EM}) cells relative to naive T cells (Figure 5E). CD8 T cells were negatively enriched for genes that have a higher expression in naive T cells relative to memory T, T_{CM}, T_{EM}, $PD1^{lo}$ (CD8 T_{EM}), and $PD1^{hi}$ (CD8 T_{EM}) cells (Figure 5E). Therefore, GSEA of CD8 T smoking DEGs identified immunological signatures indicative of an increased expression of genes associated with effector memory and central memory functions and decreased expression of genes associated with naive T cells.

CD8 T DNA Methylomes Indicate Smoking Dose-Dependent Accelerated Aging and Decreased TL

In CD8 T cells, the shift from naive to differentiated states has been associated with aging and senescence.[29] To determine whether tobacco smoke exposure was associated with immune aging and senescence, we analyzed DNA methylation data from bulk CD8 T cells (see STAR Methods). We used DNAm PhenoAge[30] to calculate age acceleration (see STAR Methods). In the donors used for scRNA-seq and mass cytometry, we found a strong association between reduced *AHRR* DNA methylation and age acceleration ($p = 0.005$, $r^2 = 0.76$; Figure 5F). Since shortened telomeres (TL) are indicative of T cell senescence, we used a DNA methylation estimator of TL (DNAmTL)[31] to estimate the TL of CD8 T cells (see STAR Methods). We found a strong association between lower *AHRR* DNA methylation and shorter DNAmTL ($p = 0.0004$, $r^2 = 0.89$; Figure 5G). To confirm these effects in a larger cohort, we analyzed CD8 T cell DNA methylation in a group of 131 individuals (Table S1). Age acceleration was highly significantly correlated with smoking dose ($p < 0.00009$), and ~11% of the variance in age acceleration in this population could be attributed to smoking dose (Figure 5H). Similarly, methylation-derived CD8 T cell TL was highly significantly associated with smoking dose ($p < 0.0002$, $r^2 = 0.11$; Figure 5I).

Smoking-Associated Gene Expression Changes in PBMC Populations

Since we did not observe substantial changes in subset distribution for the majority of PBMC populations, we compared average per-cell gene expression for all cells within each cell type (CD4 T, NKT, NK, monocyte, DC, and B) to identify smoking DEGs. For CD4 T cells, we found 1,563 DEGs—1,278 showed increased

Figure 5. CD8 T Bulk Transcriptomes Reflect Differentiation State Shifts at Single-Cell Level and DNA Methylomes Demonstrate Accelerated Aging and Shortened Telomeres

(A) Top 350 upregulated and downregulated differentially expressed genes (DEGs) between smokers (SM, n = 4) and nonsmokers (NS, n = 4) from CD8 T cells (scRNA-seq). Donors were separated by smoking status using smoking scRNA-seq-DEGs for hierarchical clustering. Labeled genes were also significantly upregulated in the CD8 T cell microarray results.

(B) Comparison of bulk RNA-seq expression of isolated CD8 T cells between smokers (n = 7) and nonsmokers (n = 8). DEGs with higher expression in smokers are labeled in red and DEGs with lower expression in smokers are denoted in blue. The gene names in black were altered in bulk RNA-seq and scRNA-seq. The gene names in gray were altered in bulk RNA-seq and microarray. The gene names in boldface were altered in microarray, bulk RNA-seq, and scRNA-seq.

(C) Principal-component analysis (PCA) of bulk RNA-seq. Donors used in both scRNA-seq and bulk RNA-seq are labeled with "F" and "V" patient codes. See Table S1 for donor information.

(D) Comparison of microarray expression of isolated CD8 T cells between smokers (n = 9) and nonsmokers (n = 10). The genes with higher expression in smokers are red and the genes with lower expression in smokers are blue. The gene names in black were altered in microarray and scRNA-seq. The gene names in gray were altered in microarray and bulk RNA-seq. The gene names in boldface were altered in microarray, bulk RNA-seq, and scRNA-seq.

(E) Immunological signatures and chemical and genetic perturbations that were significantly enriched (FWER < 0.05) by GSEA in scRNA-seq, bulk RNA-seq, and microarray.

(F–I) In CD8 T cells, age acceleration (F, H) and shortened telomeres (G, I) are correlated with the smoking dose (*AHRR* DNA methylation) in scRNA-seq donors (F–G) and a larger group (H–I) of nonsmokers (n = 71, open blue circles) and smokers (n = 60, closed red circles).

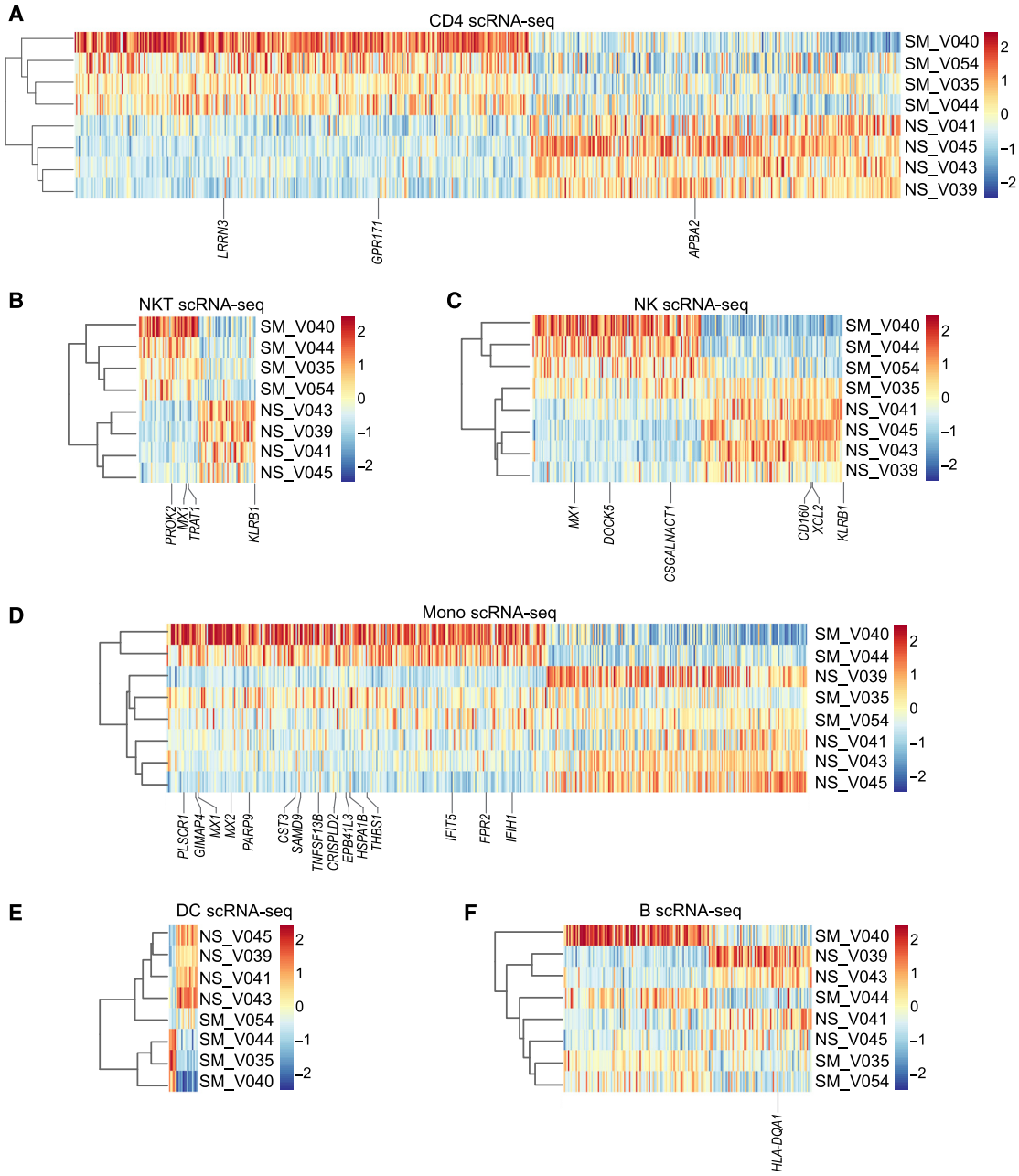

Figure 6. Major Cell Types Show Gene Expression Changes in Peripheral Blood of Smokers

(A) Hierarchical clustering of the top 350 increased and decreased DEGs between smokers (n = 4) and nonsmokers (n = 4) from CD4 T cells (scRNA-seq).
(B–F) Heatmaps of smoking DEGs (scRNA-seq) in NKT cells (B), NK cells (C), monocytes (D), DCs (E), and B cells (F).

and 285 showed decreased expression (Table S6). Hierarchical clustering of donors by CD4 T smoking DEGs clustered individuals by smoking status (Figure 6A). Bulk gene expression of isolated CD4$^+$ cells identified 2 upregulated (*LRRN3* and *GPR171*) and 1 downregulated (*APBA2*) gene in common with the CD4 T pseudobulk analysis (Figures 6A and S6A). NKT cells had 89 smoking DEGs, 45 with increased and 44 with decreased expression, and NK cells had 238 smoking DEGs, 129 with increased and 109 with decreased expression (Table S6). Hierarchical clustering of DEGs separated donors by smoking status for NKT but not for NK cells (Figures 6B and 6C). CD56$^+$ cells (bulk), which contain NKT and NK cells, shared 3 upregulated genes (*PROK2*, *MX1*, and *TRAT1*) and 1 downregulated gene (*KLRB1*) with NKT cells and 3 upregulated (*MX1*, *DOCK5*, and *CSGALNACT1*) and 3 downregulated genes (*CD160*, *XCL2*, and *KLRB1*) with NK cells (Figures 6B, 6C, and S6B). For monocytes, we found 488 DEGs between smokers and nonsmokers by scRNA pseudobulk analysis (Figure 6D; Table S6). Of the

Table 1. Smoking DEGs Altered in Both scRNA-Seq and Microarray

Gene Name	DEG		Biological Process/Function/Pathway
CD8 T			
granzyme B	↑	*GZMB*	PD-1^{low}[44]
natural killer cell granule protein 7	↑	*NKG7*	PD-1^{low}, PD-1^{high}[44]
perforin 1	↑	*PRF1*	PD-1^{low}, PD-1^{high}[44]
killer cell lectin like receptor D1	↑	*KLRD1*	PD-1^{low}, PD-1^{high}[44]
sterile α motif domain containing 3	↑	*SAMD3*	CD8 T tolerance[58,59]
G protein-coupled receptor 171	↑	***GPR171***	negative regulation of myeloid differentiation[60]
calpastatin	↑	*CAST*	PD-1^{low}, PD-1^{high};[44] effector memory, central memory[61]
chromosome 1 open reading frame 21	↑	*C1orf21*	cytotoxic T by scRNA-seq in Crohn's disease[59]
family with sequence similarity 129, member A	↑	*FAM129A*	PD-1^{low}, PD-1^{high};[44] memory, effector memory, central memory[61]
TNF superfamily member 10	↑	*TNFSF10*	marker for atherosclerosis plaque formation[62]
C-X3-C motif chemokine receptor 1	↑	*CX3CR1*	chemokine receptor associated with terminally differentiated effector CD8 cells[63]
pyrin and HIN domain family member 1	↑	*PYHIN1*	PD-1^{low}, PD-1^{high};[44] memory[61]
AT-rich interaction domain 5B	↑	*ARID5B*	central memory[61]
zinc finger E-box binding homeobox 2	↑	***ZEB2***[a]	PD-1^{low}, PD-1^{high}[44]
CD58 molecule	↑	*CD58*	PD-1^{low}, PD-1^{high};[44] memory, effector memory, central memory[61]
protein kinase cAMP-dependent type I regulatory subunit α	↑	*PRKAR1A*	enhanced cytoxicity of effector T cells[64]
acyloxyacyl hydrolase	↑	*AOAH*	effector memory phenotype, increase in chronic lymphocytic leukemia CD3 T cells[65]
proline rich 5-like	↑	*PRR5L*	PD-1^{low}, PD-1^{high};[44] effector memory, central memory[61]
MYB proto-oncogene like 1	↑	*MYBL1*	PD-1^{low}, PD-1^{high};[44] memory, effector memory, central memory[61]
ATPase plasma membrane Ca^{2+} transporting 4	↑	*ATP2B4*	PD-1^{low}, PD-1^{high};[44] memory, effector memory, central memory[61]
synaptotagmin 11	↑	*SYT11*	PD-1^{low}, PD-1^{high}[44]
killer cell Ig-like receptor, 3 Ig domains, and long cytoplasmic tail 2	↑	*KIR3DL2*[a]	T cell aging[66]
death domain containing 1	↑	*DTHD1*	unknown function
fibrinogen like 2	↑	*FGL2*[a]	replicative senescence,[67] procoagulant[68]
CD4 T			
leucine-rich repeat neuronal protein 3	↑	*LRRN3*[a]	smoking methylation,[56] T cell replicative senescence[69]
G protein-coupled receptor 171	↑	***GPR171***	negative regulation of myeloid differentiation[60]
amyloid β precursor protein binding family A member 2	↓	*APBA2*	smoking methylation[38]
NKT			
prokineticin 2	↑	*PROK2*	inflammatory response in smoking[70] and diabetes[71]
MX dynamin like GTPase 1	↑	***MX1***[a]	TNF-α induced cellular senescence[37]
T cell receptor associated transmembrane adaptor 1	↑	*TRAT1*	leukocyte activation[72]

(*Continued on next page*)

Table 1. *Continued*

Gene Name	DEG		Biological Process/Function/Pathway
killer cell lectin like receptor B1	↓	***KLRB1***[a]	downregulated in human aged $CD4^+$ memory T cells[66]
NK			
MX dynamin like GTPase 1	↑	***MX1***[a]	TNF-α induced cellular senescence[37]
dedicator of cytokinesis 5	↑	*DOCK5*[a]	upregulated in $CD57^+$ NK[73]
chondroitin sulfate N-acetylgalactosaminyltransferase 1	↑	*CSGALNACT1*	positively correlated with smoking[74]
CD160 molecule	↓	*CD160*[a]	increased in exhausted T cells[75]
X-C motif chemokine ligand 2	↓	*XCL2*	overexpressed in lung cancer tumors, increases with prognosis[76]
killer cell lectin like receptor B1	↓	***KLRB1***[a]	downregulated in human aged $CD4^+$ memory T cells[66]
Monocytes			
phospholipid scramblase 1	↑	*PLSCR1*	expression increased with cytokine treatment[77]
GTPase, IMAP family member 4	↑	*GIMAP4*	regulates INF-γ in CD4 T cell differentiation[78]
MX dynamin like GTPase 1	↑	***MX1***[a]	TNF-α-induced cellular senescence[37]
MX dynamin like GTPase 2	↑	*MX2*[a]	TNF-α-induced cellular senescence[37]
poly(ADP-ribose) polymerase family member 9	↑	*PARP9*	silences pro-inflammatory genes, found in atherosclerotic plaques[41]
cystatin C	↑	*CST3*[a]	atherosclerosis,[38] cellular senescence[39]
sterile α motif domain containing 9	↑	*SAMD9*	anti-inflammatory factor[79]
TNF superfamily member 13b	↑	*TNFSF13B*	regulates proliferation and differentiation of atherogenic B cells[40]
Cysteine-rich secretory protein LCCL domain containing 2	↑	*CRISPLD2*	regulates anti-inflammatory effects[80]
erythrocyte membrane protein band 4.1-like 3	↑	*EPB41L3*	positively correlated smoking gene and associated with cancer[74]
heat shock protein family A (Hsp70) member 1B	↑	*HSPA1B*	overexpressed in advanced atherosclerosis[42]
thrombospondin 1	↑	*THBS1*	regulation of monocyte mobility, vascular inflammation[81]
IFN-induced protein with tetratricopeptide repeats 5	↑	*IFIT5*[a]	up in TNF-α-mediated cellular senescence[37]
formyl peptide receptor 2	↑	*FPR2*	increased in atherosclerotic lesions and plaque stability[43]
IFN induced with helicase C domain 1	↑	*IFIH1*[a]	up in TNF-α-mediated cellular senescence[37]
B			
major histocompatibility complex, class II, DQ α 1	↓	*HLA-DQA1*	presents peptides from extracellular protein in T cells[82]

cAMP, cyclic AMP; CLL, XX; DEG, differentially expressed gene; GTPase, guanosine triphosphatase; INF, interferon; TNF, tumor necrosis factor.
[a]Gene associated with cellular senescence.

290 DEGs with higher expression in smokers' monocytes, 15 increased in smokers' isolated $CD14^+$ cells by microarray (Figures 6D and S6C). For DCs, we identified 21 smoking DEGs—5 showed increased and 16 showed decreased expression (Figure 6E; Table S6). In B cells, we found 190 DEGs, 111 with increased and 79 with decreased expression in smokers (Table S6). Using microarray in $CD19^+$ cells, we confirmed the decreased expression of *HLA-DQA1* in B cells from smokers compared to nonsmokers (Figures 6F and S6D). Table 1 lists the biological relevance of smoking DEGs found in PBMC populations by pseudobulk scRNA-seq and confirmed by microarray.

DISCUSSION

Our study reveals $CD16^+$ CD8 T cells and other signs of immune cell dysfunction as elevated in smokers. These cells, uncovered

by scRNA-seq and confirmed by mass cytometry in human PBMCs from multiple individuals, shared transcriptomic features with iTNK cells, which acquire NK surface receptors and have increased cytotoxic potency.[28] Combined with CD16 and CD45RA protein expression, the transcriptome of the NK-like CD8 T cells implies an innate-like, terminally differentiated CD8 T subset. CD16, commonly associated with NK cells, binds IgG antibodies to mediate antibody-dependent cellular cytotoxicity (ADCC); exogenous or endogenous CD16 expression enables T cells to execute ADCC.[26,32] Consistent with a heightened cytolytic potential, the NK-like CD8 T cells had elevated mRNA expression of cytolytic effector molecules *GZMB* and *PRF1*; these transcripts were also higher in smokers than nonsmokers within this subset. Granzyme B and perforin-expressing CD8 T cells contribute to the development of atherosclerotic plaques in mice.[33,34] As such, our results highlight a potential link between smoking-induced functional changes in human CD8 T cells and atherosclerosis.

Applying scRNA-seq and mass cytometry to PBMCs from tobacco smoke-exposed individuals, we show that major immune populations can be discerned and disparate subsets can be identified among CD4 T cells, CD8 T cells, NK cells, monocytes, and B cells. Pseudobulk analysis of immune cell populations revealed smoking DEGs, several of which were confirmed in bulk cell-type fractions. The increase in smokers' Tregs is likely masked in bulk data from isolated CD4 T cells because Tregs are a low-frequency subset. In a larger cohort of healthy women (N = 75), smoking was found to be a positive predictor of Treg levels in peripheral blood.[35] Notably, Tregs have been shown to induce T cell senescence,[36] highlighting a potential role for the increase in Tregs observed here. Senescence-related genes were altered in smokers in multiple cell types (Table 1). *MX1*, induced in tumor necrosis factor-α (TNF-α)-mediated senescence,[37] increased in smokers in NKT cells, NK cells, and monocytes.

Alluding to the shared regulation of pro-senescent and pro-atherosclerotic signaling, TNF-α-induced senescence genes are enriched for atherosclerosis signaling genes.[37] *CST3*, associated with subclinical atherosclerosis[38] and cellular senescence,[39] increased in smokers' monocytes. We also identified *TNFSF13B*, a critical regulator of atherogenic B cell proliferation and differentiation.[40] Other notable genes connected to atherosclerosis that increased in smokers' monocytes include *PARP9*,[41] *HSPA1B*,[42] and *FPR2*.[43]

Two approaches, established markers and trajectory inference, demonstrate that smokers lose naive and gain T_{CM}-like and T_{EMRA}-like cells. Differentiation state shifts in CD8 T cells were supported by bulk analysis methods. All 3 transcriptomic platforms identified changes associated with PD-1^{hi} CD8 T cells. With persistent antigen stimulation, the inhibitory effect of the PD-1 pathway contributes to pathologies associated with T cell dysfunction during chronic viral infection and tumor evasion of host immune response.[44] Duraiswamy et al.[44] demonstrated that PD-1^{hi} CD8 T cells obtained from healthy adults had gene expression profiles similar to those of PD-1^{lo} CD8 T cells and did not show either exhausted gene signatures or phenotypes characteristic of PD-1^{hi} cells obtained from humans or mice with chronic infections. Smoking DEGs found in CD8 T cells in pseudobulk scRNA-seq, bulk RNA-seq, or microarray were represented by these gene signatures (Figure 5E; Table 1). Notably, bulk RNA-seq data were acquired from prior visits from donors used for scRNA-seq, indicating a chronic or recurring state of activation in smokers' CD8 T cells. Chronic activation suggests that CD8 T cells obtained from healthy smokers here may represent a dysfunctional phenotype.

Consistent with an end-stage T_{EMRA} phenotype, NK-like CD8 T cells had the latest pseudotimes. *GFI1*, a transcriptional repressor of interleukin-7 receptor α (IL-7Rα) that drives the terminal differentiation of CD8 T cells,[45] was elevated in NK-like CD8 T_{EMRA} cells. The loss of naive and accumulation of terminally differentiated T cells, observed here in smokers, mimics the altered distribution of T cell subsets reported in aging and chronic infection that is proposed to result from repeated or persistent stimulation of immune cells, ultimately leading to the loss of immune function either due to replicative senescence or functional exhaustion.[46-48] Gene expression changes in low-frequency subsets may not be discernible in pseudobulk and bulk analyses. Therefore, we looked for indicators of T cell dysfunction within the smoking-associated NK-like CD8 T_{EMRA} subset. While *TOX*, a transcription factor that controls fate commitment in exhausted T cells,[49] was elevated in smokers' NK-like CD8 T_{EMRA} cells compared to other CD8 T cells, it was only detected in 8.9% of cells within this cluster. Other exhaustion markers *PDCD1*, *CTLA4*, and *HAVCR2* were not increased. Whereas exhausted CD8 T cells lack cytotoxic activity, the high expression of genes encoding proteins responsible for cytolytic activity in NK-like CD8 T_{EMRA} cells suggests that these cells more likely represent a senescent or pre-senescent state. In support, compared to other CD8 T cells, the NK-like CD8 T_{EMRA} cells from both smokers and nonsmokers had an elevated expression of *KLRG1*, an inhibitory receptor correlated with extensive proliferative history,[50] and *B3GAT1* (CD57), a marker of limited proliferative potential and shortened telomeres.[51] Senescence is induced as the result of telomere shortening or nontelomeric DNA damage,[46] both of which have been reported to occur in smokers.[52,53]

To further examine the effects of smoking on immune aging and senescence in CD8 T cells, we used DNA methylation-based models to demonstrate that age acceleration and reduced TL correlated with smoking dose. Accelerated immune system aging accompanies T cell senescence and can manifest as impaired immunological memory,[54] which could contribute to attenuated immune responses in smokers.

In addition to impaired immune function, prolonged SASP, driven by the accumulation of senescent cells, can lead to chronic inflammation.[29] Callender et al.[17] showed that CD8 T_{EMRA} cells exhibit both inflammatory and senescent phenotypes. Consistent with SASP, *TNFSF10* (secreted factor) and *CX3CR1* (chemokine receptor) were increased in smokers' CD8 T cells, and NK-like CD8 T_{EMRA} cells expressed secreted factors *CTSW* and *PRSS23*. The *PRSS23* methylation level is a reproducible biomarker of tobacco smoke exposure,[55-57] and altered methylation persists up to at least 30 years after smoking cessation.[15,16] This indicates that epigenetic modifications likely contribute to the senescent attributes of CD8 T cells in smokers. The acquisition of CD16 and NK-like characteristics implies an underappreciated role for CD16 receptor in the maintenance of cytotoxic activity in T_{EMRA} cells in smokers.

In conclusion, we show an association between smoking and an immune-cell subtype that can be isolated to investigate how NK-like CD8 T_{EMRA} cells contribute to proinflammatory states in smoking-mediated chronic inflammatory conditions. Our data illustrate links between smoking-induced gene expression changes and a T cell senescent phenotype, immune system aging, and, potentially, atherosclerosis. Consequently, our use of recently developed single-cell technologies to address tobacco smoke exposure has great potential to affect global health.

Limitations of Study

The single-cell approaches have low sample numbers. Reproducing our current findings in a larger group and additional characterization of CMV status will refine the roles of smoking and CMV in CD8 T cell aging. In addition, functional studies are needed to determine the importance of the immune cell changes reported here.

STAR★METHODS

Detailed methods are provided in the online version of this paper and include the following:

- KEY RESOURCES TABLE
- RESOURCE AVAILABILITY
  - Lead Contact
  - Materials Availability
  - Data and Code Availability
- EXPERIMENTAL MODEL AND SUBJECT DETAILS
  - Human Subjects
- METHOD DETAILS
  - PBMC Isolation for scRNA-seq and Mass Cytometry
  - PBMC Preparation for Purified Cell Fractions
  - Mass Cytometry
  - Preparation of Sequencing Libraries
  - Microarray
  - DNA Methylation arrays
- QUANTIFICATION AND STATISTICAL ANALYSIS
  - Mass Cytometry Gating Strategy and Analysis
  - scRNA-seq Processing and Analysis
  - Bulk RNA-seq Analysis
  - Microarray Analysis
  - GSEA
  - DNA Methylation Processing and Analysis
  - Reanalysis of Microarray Data

SUPPLEMENTAL INFORMATION

Supplemental Information can be found online at https://doi.org/10.1016/j.xcrm.2020.100054.

ACKNOWLEDGMENTS

This work was funded by the Intramural Research Program of the National Institute of Environmental Health Sciences-National Institutes of Health (Z01-ES100475) and a grant from the NIH/Food and Drug Administration (FDA) Intramural Center for Tobacco Research, to D.A.B. We thank the National Institute of Environmental Health Sciences (NIEHS) Clinical Research Unit (CRU) and individuals at NIEHS: Dr. Brian Papas (Integrative Bioinformatics Support Group), Marie Iannone (Flow Cytometry Center), Laura Wharey (Molecular Genomics Core), and Nicole Reeves and Jason Malphurs (Epigenomics and DNA Sequencing Core). We also thank Leonardo Albertini-Sanchez for manuscript comments.

AUTHOR CONTRIBUTIONS

D.A.B., M.R.C., S.N.M., M.W., and G.S.P. designed the study and were involved in donor selection. M.R.C., S.N.M., and I.J.B.T. performed the experiments. S.N.M., M.R.C., O.A.L., X.W., and B.D.B. analyzed the data. S.N.M., M.R.C., and D.A.B. interpreted the data and wrote the paper, with input from O.A.L.

DECLARATION OF INTERESTS

The authors declare no competing interests.

Received: December 3, 2019
Revised: April 14, 2020
Accepted: June 23, 2020
Published: July 21, 2020

REFERENCES

1. World Health Organization (2015). WHO global report on trends in prevalence of tobacco smoking 2015. https://apps.who.int/iris/handle/10665/156262.
2. Stämpfli, M.R., and Anderson, G.P. (2009). How cigarette smoke skews immune responses to promote infection, lung disease and cancer. Nat. Rev. Immunol. *9*, 377–384.
3. Hansson, G.K. (2005). Inflammation, atherosclerosis, and coronary artery disease. N. Engl. J. Med. *352*, 1685–1695.
4. Ilhan, F., and Kalkanli, S.T. (2015). Atherosclerosis and the role of immune cells. World J. Clin. Cases *3*, 345–352.
5. Su, D., Wang, X., Campbell, M.R., Porter, D.K., Pittman, G.S., Bennett, B.D., Wan, M., Englert, N.A., Crowl, C.L., Gimple, R.N., et al. (2016). Distinct Epigenetic Effects of Tobacco Smoking in Whole Blood and among Leukocyte Subtypes. PLOS ONE *11*, e0166486.
6. Wan, M., Bennett, B.D., Pittman, G.S., Campbell, M.R., Reynolds, L.M., Porter, D.K., Crowl, C.L., Wang, X., Su, D., Englert, N.A., et al. (2018). Identification of Smoking-Associated Differentially Methylated Regions Using Reduced Representation Bisulfite Sequencing and Cell type-Specific Enhancer Activation and Gene Expression. Environ. Health Perspect. *126*, 047015.
7. Reynolds, L.M., Lohman, K., Pittman, G.S., Barr, R.G., Chi, G.C., Kaufman, J., Wan, M., Bell, D.A., Blaha, M.J., Rodriguez, C.J., and Liu, Y. (2017). Tobacco exposure-related alterations in DNA methylation and gene expression in human monocytes: the Multi-Ethnic Study of Atherosclerosis (MESA). Epigenetics *12*, 1092–1100.
8. Wang, Y., Shu, Y., Xiao, Y., Wang, Q., Kanekura, T., Li, Y., Wang, J., Zhao, M., Lu, Q., and Xiao, R. (2014). Hypomethylation and overexpression of ITGAL (CD11a) in CD4(+) T cells in systemic sclerosis. Clin. Epigenetics *6*, 25.
9. Florescu, A., Ferrence, R., Einarson, T., Selby, P., Soldin, O., and Koren, G. (2009). Methods for quantification of exposure to cigarette smoking and environmental tobacco smoke: focus on developmental toxicology. Ther. Drug Monit. *31*, 14–30.
10. Butler, A., Hoffman, P., Smibert, P., Papalexi, E., and Satija, R. (2018). Integrating single-cell transcriptomic data across different conditions, technologies, and species. Nat. Biotechnol. *36*, 411–420.
11. Stuart, T., Butler, A., Hoffman, P., Hafemeister, C., Papalexi, E., Mauck, W.M., 3rd, Hao, Y., Stoeckius, M., Smibert, P., and Satija, R. (2019). Comprehensive Integration of Single-Cell Data. Cell *177*, 1888–1902.
12. Finak, G., McDavid, A., Yajima, M., Deng, J., Gersuk, V., Shalek, A.K., Slichter, C.K., Miller, H.W., McElrath, M.J., Prlic, M., et al. (2015). MAST:

a flexible statistical framework for assessing transcriptional changes and characterizing heterogeneity in single-cell RNA sequencing data. Genome Biol. *16*, 278.

13. Kotecha, N., Krutzik, P.O., and Irish, J.M. (2010). Web-based analysis and publication of flow cytometry experiments. Curr. Protoc. Cytom. *53*, 10.17.1–10.17.24.
14. Samusik, N., Good, Z., Spitzer, M.H., Davis, K.L., and Nolan, G.P. (2016). Automated mapping of phenotype space with single-cell data. Nat. Methods *13*, 493–496.
15. Joehanes, R., Just, A.C., Marioni, R.E., Pilling, L.C., Reynolds, L.M., Mandaviya, P.R., Guan, W., Xu, T., Elks, C.E., Aslibekyan, S., et al. (2016). Epigenetic Signatures of Cigarette Smoking. Circ. Cardiovasc. Genet. *9*, 436–447.
16. Zeilinger, S., Kühnel, B., Klopp, N., Baurecht, H., Kleinschmidt, A., Gieger, C., Weidinger, S., Lattka, E., Adamski, J., Peters, A., et al. (2013). Tobacco smoking leads to extensive genome-wide changes in DNA methylation. PLOS ONE *8*, e63812.
17. Callender, L.A., Carroll, E.C., Beal, R.W.J., Chambers, E.S., Nourshargh, S., Akbar, A.N., and Henson, S.M. (2018). Human $CD8^+$ EMRA T cells display a senescence-associated secretory phenotype regulated by p38 MAPK. Aging Cell *17*, e12675.
18. Martins, G.A., Cimmino, L., Liao, J., Magnusdottir, E., and Calame, K. (2008). Blimp-1 directly represses Il2 and the Il2 activator Fos, attenuating T cell proliferation and survival. J. Exp. Med. *205*, 1959–1965.
19. Shaulian, E., and Karin, M. (2002). AP-1 as a regulator of cell life and death. Nat. Cell Biol. *4*, E131–E136.
20. Omilusik, K.D., Best, J.A., Yu, B., Goossens, S., Weidemann, A., Nguyen, J.V., Seuntjens, E., Stryjewska, A., Zweier, C., Roychoudhuri, R., et al. (2015). Transcriptional repressor ZEB2 promotes terminal differentiation of CD8+ effector and memory T cell populations during infection. J. Exp. Med. *212*, 2027–2039.
21. Scott, C.L., and Omilusik, K.D. (2019). ZEBs: Novel Players in Immune Cell Development and Function. Trends Immunol. *40*, 431–446.
22. Street, K., Risso, D., Fletcher, R.B., Das, D., Ngai, J., Yosef, N., Purdom, E., and Dudoit, S. (2018). Slingshot: cell lineage and pseudotime inference for single-cell transcriptomics. BMC Genomics *19*, 477.
23. Jackson, S.E., Sedikides, G.X., Okecha, G., Poole, E.L., Sinclair, J.H., and Wills, M.R. (2017). Latent Cytomegalovirus (CMV) Infection Does Not Detrimentally Alter T Cell Responses in the Healthy Old, But Increased Latent CMV Carriage Is Related to Expanded CMV-Specific T Cells. Front. Immunol. *8*, 733.
24. Jackson, S.E., Sedikides, G.X., Okecha, G., and Wills, M.R. (2019). Generation, maintenance and tissue distribution of T cell responses to human cytomegalovirus in lytic and latent infection. Med. Microbiol. Immunol. (Berl.) *208*, 375–389.
25. Björkström, N.K., Gonzalez, V.D., Malmberg, K.J., Falconer, K., Alaeus, A., Nowak, G., Jorns, C., Ericzon, B.G., Weiland, O., Sandberg, J.K., and Ljunggren, H.G. (2008). Elevated numbers of Fc gamma RIIIA+ (CD16+) effector CD8 T cells with NK cell-like function in chronic hepatitis C virus infection. J. Immunol. *181*, 4219–4228.
26. Clémenceau, B., Vivien, R., Berthomé, M., Robillard, N., Garand, R., Gallot, G., Vollant, S., and Vié, H. (2008). Effector memory alphabeta T lymphocytes can express FcgammaRIIIa and mediate antibody-dependent cellular cytotoxicity. J. Immunol. *180*, 5327–5334.
27. Clémenceau, B., Vivien, R., Debeaupuis, E., Esbelin, J., Biron, C., Levy, Y., and Vié, H. (2011). FcγRIIIa (CD16) induction on human T lymphocytes and CD16pos T-lymphocyte amplification. J. Immunother. *34*, 542–549.
28. Li, P., Burke, S., Wang, J., Chen, X., Ortiz, M., Lee, S.C., Lu, D., Campos, L., Goulding, D., Ng, B.L., et al. (2010). Reprogramming of T cells to natural killer-like cells upon Bcl11b deletion. Science *329*, 85–89.
29. Goronzy, J.J., and Weyand, C.M. (2019). Mechanisms underlying T cell ageing. Nat. Rev. Immunol. *19*, 573–583.
30. Levine, M.E., Lu, A.T., Quach, A., Chen, B.H., Assimes, T.L., Bandinelli, S., Hou, L., Baccarelli, A.A., Stewart, J.D., Li, Y., et al. (2018). An epigenetic biomarker of aging for lifespan and healthspan. Aging (Albany N.Y.) *10*, 573–591.
31. Lu, A.T., Seeboth, A., Tsai, P.C., Sun, D., Quach, A., Reiner, A.P., Kooperberg, C., Ferrucci, L., Hou, L., Baccarelli, A.A., et al. (2019). DNA methylation-based estimator of telomere length. Aging (Albany N.Y.) *11*, 5895–5923.
32. Clémenceau, B., Congy-Jolivet, N., Gallot, G., Vivien, R., Gaschet, J., Thibault, G., and Vié, H. (2006). Antibody-dependent cellular cytotoxicity (ADCC) is mediated by genetically modified antigen-specific human T lymphocytes. Blood *107*, 4669–4677.
33. Kyaw, T., Winship, A., Tay, C., Kanellakis, P., Hosseini, H., Cao, A., Li, P., Tipping, P., Bobik, A., and Toh, B.H. (2013). Cytotoxic and proinflammatory CD8+ T lymphocytes promote development of vulnerable atherosclerotic plaques in apoE-deficient mice. Circulation *127*, 1028–1039.
34. Hiebert, P.R., Boivin, W.A., Zhao, H., McManus, B.M., and Granville, D.J. (2013). Perforin and granzyme B have separate and distinct roles during atherosclerotic plaque development in apolipoprotein E knockout mice. PLOS ONE *8*, e78939.
35. Hampras, S.S., Nesline, M., Wallace, P.K., Odunsi, K., Furlani, N., Davis, W., and Moysich, K.B. (2012). Predictors of immunosuppressive regulatory T lymphocytes in healthy women. J. Cancer Epidemiol. *2012*, 191090.
36. Ye, J., Huang, X., Hsueh, E.C., Zhang, Q., Ma, C., Zhang, Y., Varvares, M.A., Hoft, D.F., and Peng, G. (2012). Human regulatory T cells induce T-lymphocyte senescence. Blood *120*, 2021–2031.
37. Kandhaya-Pillai, R., Miro-Mur, F., Alijotas-Reig, J., Tchkonia, T., Kirkland, J.L., and Schwartz, S. (2017). TNFα-senescence initiates a STAT-dependent positive feedback loop, leading to a sustained interferon signature, DNA damage, and cytokine secretion. Aging (Albany N.Y.) *9*, 2411–2435.
38. Chung, Y.K., Lee, Y.J., Kim, K.W., Cho, R.K., Chung, S.M., Moon, J.S., Yoon, J.S., Won, K.C., and Lee, H.W. (2018). Serum cystatin C is associated with subclinical atherosclerosis in patients with type 2 diabetes: a retrospective study. Diab. Vasc. Dis. Res. *15*, 24–30.
39. Basisty, N., Kale, A., Jeon, O.H., Kuehnemann, C., Payne, T., Rao, C., Holtz, A., Shah, S., Sharma, V., Ferrucci, L., et al. (2020). A Proteomic Atlas of Senescence-Associated Secretomes for Aging Biomarker Development. PLOS Biol. *18*, e3000599.
40. Kyaw, T., Cui, P., Tay, C., Kanellakis, P., Hosseini, H., Liu, E., Rolink, A.G., Tipping, P., Bobik, A., and Toh, B.H. (2013). BAFF receptor mAb treatment ameliorates development and progression of atherosclerosis in hyperlipidemic ApoE(-/-) mice. PLOS ONE *8*, e60430.
41. Iwata, H., Goettsch, C., Sharma, A., Ricchiuto, P., Goh, W.W., Halu, A., Yamada, I., Yoshida, H., Hara, T., Wei, M., et al. (2016). PARP9 and PARP14 cross-regulate macrophage activation via STAT1 ADP-ribosylation. Nat. Commun. *7*, 12849.
42. Kilic, A., and Mandal, K. (2012). Heat shock proteins: pathogenic role in atherosclerosis and potential therapeutic implications. Autoimmune Dis. *2012*, 502813.
43. Petri, M.H., Laguna-Fernández, A., Gonzalez-Diez, M., Paulsson-Berne, G., Hansson, G.K., and Bäck, M. (2015). The role of the FPR2/ALX receptor in atherosclerosis development and plaque stability. Cardiovasc. Res. *105*, 65–74.
44. Duraiswamy, J., Ibegbu, C.C., Masopust, D., Miller, J.D., Araki, K., Doho, G.H., Tata, P., Gupta, S., Zilliox, M.J., Nakaya, H.I., et al. (2011). Phenotype, function, and gene expression profiles of programmed death-1(hi) CD8 T cells in healthy human adults. J. Immunol. *186*, 4200–4212.
45. Ligons, D.L., Tuncer, C., Linowes, B.A., Akcay, I.M., Kurtulus, S., Deniz, E., Atasever Arslan, B., Cevik, S.I., Keller, H.R., Luckey, M.A., et al. (2012). CD8 lineage-specific regulation of interleukin-7 receptor expression by the transcriptional repressor Gfi1. J. Biol. Chem. *287*, 34386–34399.

46. Akbar, A.N., and Henson, S.M. (2011). Are senescence and exhaustion intertwined or unrelated processes that compromise immunity? Nat. Rev. Immunol. *11*, 289–295.

47. Larbi, A., and Fulop, T. (2014). From "truly naïve" to "exhausted senescent" T cells: when markers predict functionality. Cytometry A *85*, 25–35.

48. Reiser, J., and Banerjee, A. (2016). Effector, Memory, and Dysfunctional CD8(+) T Cell Fates in the Antitumor Immune Response. J. Immunol. Res. *2016*, 8941260.

49. Khan, O., Giles, J.R., McDonald, S., Manne, S., Ngiow, S.F., Patel, K.P., Werner, M.T., Huang, A.C., Alexander, K.A., Wu, J.E., et al. (2019). TOX transcriptionally and epigenetically programs $CD8^+$ T cell exhaustion. Nature *571*, 211–218.

50. Voehringer, D., Blaser, C., Brawand, P., Raulet, D.H., Hanke, T., and Pircher, H. (2001). Viral infections induce abundant numbers of senescent CD8 T cells. J. Immunol. *167*, 4838–4843.

51. Brenchley, J.M., Karandikar, N.J., Betts, M.R., Ambrozak, D.R., Hill, B.J., Crotty, L.E., Casazza, J.P., Kuruppu, J., Migueles, S.A., Connors, M., et al. (2003). Expression of CD57 defines replicative senescence and antigen-induced apoptotic death of CD8+ T cells. Blood *101*, 2711–2720.

52. Song, Z., von Figura, G., Liu, Y., Kraus, J.M., Torrice, C., Dillon, P., Rudolph-Watabe, M., Ju, Z., Kestler, H.A., Sanoff, H., and Lenhard Rudolph, K. (2010). Lifestyle impacts on the aging-associated expression of biomarkers of DNA damage and telomere dysfunction in human blood. Aging Cell *9*, 607–615.

53. Valdes, A.M., Andrew, T., Gardner, J.P., Kimura, M., Oelsner, E., Cherkas, L.F., Aviv, A., and Spector, T.D. (2005). Obesity, cigarette smoking, and telomere length in women. Lancet *366*, 662–664.

54. Reading, J.L., Gálvez-Cancino, F., Swanton, C., Lladser, A., Peggs, K.S., and Quezada, S.A. (2018). The function and dysfunction of memory $CD8^+$ T cells in tumor immunity. Immunol. Rev. *283*, 194–212.

55. Besingi, W., and Johansson, A. (2014). Smoke-related DNA methylation changes in the etiology of human disease. Hum. Mol. Genet. *23*, 2290–2297.

56. Guida, F., Sandanger, T.M., Castagné, R., Campanella, G., Polidoro, S., Palli, D., Krogh, V., Tumino, R., Sacerdote, C., Panico, S., et al. (2015). Dynamics of smoking-induced genome-wide methylation changes with time since smoking cessation. Hum. Mol. Genet. *24*, 2349–2359.

57. Joubert, B.R., Felix, J.F., Yousefi, P., Bakulski, K.M., Just, A.C., Breton, C., Reese, S.E., Markunas, C.A., Richmond, R.C., Xu, C.J., et al. (2016). DNA Methylation in Newborns and Maternal Smoking in Pregnancy: Genome-wide Consortium Meta-analysis. Am. J. Hum. Genet. *98*, 680–696.

58. Schietinger, A., Delrow, J.J., Basom, R.S., Blattman, J.N., and Greenberg, P.D. (2012). Rescued tolerant CD8 T cells are preprogrammed to reestablish the tolerant state. Science *335*, 723–727.

59. Uniken Venema, W.T., Voskuil, M.D., Vich Vila, A., van der Vries, G., Jansen, B.H., Jabri, B., Faber, K.N., Dijkstra, G., Xavier, R.J., Wijmenga, C., et al. (2019). Single-Cell RNA Sequencing of Blood and Ileal T Cells From Patients With Crohn's Disease Reveals Tissue-Specific Characteristics and Drug Targets. Gastroenterology *156*, 812–815.e22.

60. Rossi, L., Lemoli, R.M., and Goodell, M.A. (2013). Gpr171, a putative P2Y-like receptor, negatively regulates myeloid differentiation in murine hematopoietic progenitors. Exp. Hematol. *41*, 102–112.

61. Abbas, A.R., Wolslegel, K., Seshasayee, D., Modrusan, Z., and Clark, H.F. (2009). Deconvolution of blood microarray data identifies cellular activation patterns in systemic lupus erythematosus. PLOS ONE *4*, e6098.

62. Arcidiacono, M.V., Rimondi, E., Maietti, E., Melloni, E., Tisato, V., Gallo, S., Valdivielso, J.M., Fernández, E., Betriu, À., Voltan, R., et al. (2018). Relationship between low levels of circulating TRAIL and atheromatosis progression in patients with chronic kidney disease. PLOS ONE *13*, e0203716.

63. Gerlach, C., Moseman, E.A., Loughhead, S.M., Alvarez, D., Zwijnenburg, A.J., Waanders, L., Garg, R., de la Torre, J.C., and von Andrian, U.H. (2016). The Chemokine Receptor CX3CR1 Defines Three Antigen-Experienced CD8 T Cell Subsets with Distinct Roles in Immune Surveillance and Homeostasis. Immunity *45*, 1270–1284.

64. Panya, A., Thepmalee, C., Sawasdee, N., Sujjitjoon, J., Phanthaphol, N., Junking, M., Wongkham, S., and Yenchitsomanus, P.T. (2018). Cytotoxic activity of effector T cells against cholangiocarcinoma is enhanced by self-differentiated monocyte-derived dendritic cells. Cancer Immunol. Immunother. *67*, 1579–1588.

65. Göthert, J.R., Eisele, L., Klein-Hitpass, L., Weber, S., Zesewitz, M.L., Sellmann, L., Röth, A., Pircher, H., Dührsen, U., and Dürig, J. (2013). Expanded CD8+ T cells of murine and human CLL are driven into a senescent KLRG1+ effector memory phenotype. Cancer Immunol. Immunother. *62*, 1697–1709.

66. Chen, G., Lustig, A., and Weng, N.P. (2013). T cell aging: a review of the transcriptional changes determined from genome-wide analysis. Front. Immunol. *4*, 121.

67. Binet, R., Ythier, D., Robles, A.I., Collado, M., Larrieu, D., Fonti, C., Brambilla, E., Brambilla, C., Serrano, M., Harris, C.C., and Pedeux, R. (2009). WNT16B is a new marker of cellular senescence that regulates p53 activity and the phosphoinositide 3-kinase/AKT pathway. Cancer Res. *69*, 9183–9191.

68. Hu, J., Yan, J., Rao, G., Latha, K., Overwijk, W.W., Heimberger, A.B., and Li, S. (2016). The Duality of Fgl2 - Secreted Immune Checkpoint Regulator Versus Membrane-Associated Procoagulant: Therapeutic Potential and Implications. Int. Rev. Immunol. *35*, 325–339.

69. Chou, J.P., Ramirez, C.M., Wu, J.E., and Effros, R.B. (2013). Accelerated aging in HIV/AIDS: novel biomarkers of senescent human CD8+ T cells. PLOS ONE *8*, e64702.

70. Yun, J.H., Morrow, J., Owen, C.A., Qiu, W., Glass, K., Lao, T., Jiang, Z., Perrella, M.A., Silverman, E.K., Zhou, X., and Hersh, C.P. (2017). Transcriptomic Analysis of Lung Tissue from Cigarette Smoke-Induced Emphysema Murine Models and Human Chronic Obstructive Pulmonary Disease Show Shared and Distinct Pathways. Am. J. Respir. Cell Mol. Biol. *57*, 47–58.

71. Castelli, M., Amodeo, G., Negri, L., Lattanzi, R., Maftei, D., Gotti, C., Pistillo, F., Onnis, V., Congu, C., Panerai, A.E., et al. (2016). Antagonism of the Prokineticin System Prevents and Reverses Allodynia and Inflammation in a Mouse Model of Diabetes. PLOS ONE *11*, e0146259.

72. Taylor, J., Reynolds, L., Hou, L., Lohman, K., Cui, W., Kritchevsky, S., McCall, C., and Liu, Y. (2017). Transcriptomic profiles of aging in naïve and memory $CD4^+$ cells from mice. Immun. Ageing *14*, 15.

73. Lopez-Vergès, S., Milush, J.M., Pandey, S., York, V.A., Arakawa-Hoyt, J., Pircher, H., Norris, P.J., Nixon, D.F., and Lanier, L.L. (2010). CD57 defines a functionally distinct population of mature NK cells in the human CD56dimCD16+ NK-cell subset. Blood *116*, 3865–3874.

74. Charlesworth, J.C., Curran, J.E., Johnson, M.P., Göring, H.H., Dyer, T.D., Diego, V.P., Kent, J.W., Jr., Mahaney, M.C., Almasy, L., MacCluer, J.W., et al. (2010). Transcriptomic epidemiology of smoking: the effect of smoking on gene expression in lymphocytes. BMC Med. Genomics *3*, 29.

75. Kasakovski, D., Xu, L., and Li, Y. (2018). T cell senescence and CAR-T cell exhaustion in hematological malignancies. J. Hematol. Oncol. *11*, 91.

76. Zhou, H., Brekman, A., Zuo, W.L., Ou, X., Shaykhiev, R., Agosto-Perez, F.J., Wang, R., Walters, M.S., Salit, J., Strulovici-Barel, Y., et al. (2016). POU2AF1 Functions in the Human Airway Epithelium To Regulate Expression of Host Defense Genes. J. Immunol. *196*, 3159–3167.

77. Kodigepalli, K.M., Bowers, K., Sharp, A., and Nanjundan, M. (2015). Roles and regulation of phospholipid scramblases. FEBS Lett. *589*, 3–14.

78. Heinonen, M.T., Kanduri, K., Lähdesmäki, H.J., Lahesmaa, R., and Henttinen, T.A. (2015). Tubulin- and actin-associating GIMAP4 is required for IFN-γ secretion during Th cell differentiation. Immunol. Cell Biol. *93*, 158–166.

79. He, P., Wu, L.F., Bing, P.F., Xia, W., Wang, L., Xie, F.F., Lu, X., Lei, S.F., and Deng, F.Y. (2019). SAMD9 is a (epi-) genetically regulated anti-inflammatory factor activated in RA patients. Mol. Cell. Biochem. *456*, 135–144.

80. Himes, B.E., Jiang, X., Wagner, P., Hu, R., Wang, Q., Klanderman, B., Whitaker, R.M., Duan, Q., Lasky-Su, J., Nikolos, C., et al. (2014). RNA-Seq transcriptome profiling identifies CRISPLD2 as a glucocorticoid responsive gene that modulates cytokine function in airway smooth muscle cells. PLOS ONE *9*, e99625.

81. Liu, Z., Morgan, S., Ren, J., Wang, Q., Annis, D.S., Mosher, D.F., Zhang, J., Sorenson, C.M., Sheibani, N., and Liu, B. (2015). Thrombospondin-1 (TSP1) contributes to the development of vascular inflammation by regulating monocytic cell motility in mouse models of abdominal aortic aneurysm. Circ. Res. *117*, 129–141.

82. Zajacova, M., Kotrbova-Kozak, A., and Cerna, M. (2018). Expression of HLA-DQA1 and HLA-DQB1 genes in B lymphocytes, monocytes and whole blood. Int. J. Immunogenet. *45*, 128–137.

83. Subramanian, A., Tamayo, P., Mootha, V.K., Mukherjee, S., Ebert, B.L., Gillette, M.A., Paulovich, A., Pomeroy, S.L., Golub, T.R., Lander, E.S., and Mesirov, J.P. (2005). Gene set enrichment analysis: a knowledge-based approach for interpreting genome-wide expression profiles. Proc. Natl. Acad. Sci. USA *102*, 15545–15550.

84. Mootha, V.K., Lindgren, C.M., Eriksson, K.F., Subramanian, A., Sihag, S., Lehar, J., Puigserver, P., Carlsson, E., Ridderstråle, M., Laurila, E., et al. (2003). PGC-1alpha-responsive genes involved in oxidative phosphorylation are coordinately downregulated in human diabetes. Nat. Genet. *34*, 267–273.

85. Reich, M., Liefeld, T., Gould, J., Lerner, J., Tamayo, P., and Mesirov, J.P. (2006). GenePattern 2.0. Nat. Genet. *38*, 500–501.

86. Barrett, T., Wilhite, S.E., Ledoux, P., Evangelista, C., Kim, I.F., Tomashevsky, M., Marshall, K.A., Phillippy, K.H., Sherman, P.M., Holko, M., et al. (2013). NCBI GEO: archive for functional genomics data sets–update. Nucleic Acids Res. *41*, D991–D995.

87. Aryee, M.J., Jaffe, A.E., Corrada-Bravo, H., Ladd-Acosta, C., Feinberg, A.P., Hansen, K.D., and Irizarry, R.A. (2014). Minfi: a flexible and comprehensive Bioconductor package for the analysis of Infinium DNA methylation microarrays. Bioinformatics *30*, 1363–1369.

88. Fortin, J.P., Triche, T.J., Jr., and Hansen, K.D. (2017). Preprocessing, normalization and integration of the Illumina HumanMethylationEPIC array with minfi. Bioinformatics *33*, 558–560.

89. Kimball, A.K., Oko, L.M., Bullock, B.L., Nemenoff, R.A., van Dyk, L.F., and Clambey, E.T. (2018). A Beginner's Guide to Analyzing and Visualizing Mass Cytometry Data. J. Immunol. *200*, 3–22.

90. Lozoya, O.A., Santos, J.H., and Woychik, R.P. (2018). A Leveraged Signal-to-Noise Ratio (LSTNR) Method to Extract Differentially Expressed Genes and Multivariate Patterns of Expression From Noisy and Low-Replication RNAseq Data. Front. Genet. *9*, 176.

91. Benjamini, Y., and Hochberg, Y. (1995). Controlling the False Discovery Rate: A Practical and Powerful Approach to Multiple Testing. J. R. Stat. Soc. B *57*, 289–300.

92. Godec, J., Tan, Y., Liberzon, A., Tamayo, P., Bhattacharya, S., Butte, A.J., Mesirov, J.P., and Haining, W.N. (2016). Compendium of Immune Signatures Identifies Conserved and Species-Specific Biology in Response to Inflammation. Immunity *44*, 194–206.

93. Smyth, G.K. (2005). limma: linear models for microarray data. In Bioinformatics and Computational Biology Solutions Using R and Bioconductor, R. Gentleman, V.J. Carey, W. Huber, R.A. Irizarry, and S. Dudoit, eds. (Springer), pp. 397–420.

94. Smyth, G.K. (2004). Linear models and empirical Bayes methods for assessing differential expression in microarray experiments. Stat. Appl. Genet. Mol. Biol. *3*, Article3.

STAR★METHODS

KEY RESOURCES TABLE

REAGENT or RESOURCE	SOURCE	IDENTIFIER
Antibodies		
CD45 (clone HI30) 89Y	Fluidigm	Cat# 3089003; RRID: AB_2661851
CD235ab (clone HIR2) 141Pr	Fluidigm	Cat# 3141001B; RRID: AB_2651154
CD19 (clone HIB19) 142Nd	Fluidigm	Cat# 3142001; RRID: AB_2651155
CD4 (clone RPA-T4) 145Nd	Fluidigm	Cat# 3145001; RRID: AB_2661789
CD8a (clone RPA-T8) 146Nd	Fluidigm	Cat# 3146001; RRID: AB_2687641
CD7 (clone CD7-6B7) 147Sm	Fluidigm	Cat# 3147006; RRID: AB_2802104
CD66 (clone CD66a-B1.1) 149Sm	Fluidigm	Cat# 3149008; RRID: AB_2802105
CD61 (clone VI-PL2) 150Nd	Fluidigm	Cat# 3150001; RRID: AB_2661793
CD123 (clone 6H6) 151Eu	Fluidigm	Cat# 3151001; RRID: AB_2661794
CD36 (clone 5-271) 152Sm	Fluidigm	Cat# 3152007; RRID: AB_2802106
CD45RA (clone H100) 153Eu	Fluidigm	Cat# 3153001; RRID: AB_2802108
CD163 (clone GHI/61) 154Sm	Fluidigm	Cat# 3154007; RRID: AB_2661797
CD10 (clone HI10a) 156Gd	Fluidigm	Cat# 3156001; RRID: AB_2802107
CD11c (clone Bu15) 159Tb	Fluidigm	Cat# 3159001; RRID: AB_2661800
CD14 (clone M5E2) 160Gd	Fluidigm	Cat# 3160001; RRID: AB_2687634
CD16 (clone 3G8) 165Ho	Fluidigm	Cat# 3165001; RRID: AB_2802109
CD34 (clone 581) 166Er	Fluidigm	Cat# 3166012; RRID: AB_2756424
CD38 (clone HIT2) 167Er	Fluidigm	Cat# 3167001; RRID: AB_2802110
CD206 (clone 15-2) 168Er	Fluidigm	Cat# 3168008; RRID: AB_2661805
CD33 (clone WM53) 169Tm	Fluidigm	Cat# 3169010; RRID: AB_2802111
CD3 (clone UCHT1) 170Er	Fluidigm	Cat# 3170001; RRID: AB_2661807
CD20 (clone 2H7) 171Yb	Fluidigm	Cat# 3171012; RRID: AB_2802112
CD15 (clone W6D3) 172Yb	Fluidigm	Cat# 3172021; RRID: AB_2802113
HLA-DR (clone L243) 174Yb	Fluidigm	Cat# 3174001; RRID: AB_2665397
CD56 (clone NCAM 16.2) 176Yb	Fluidigm	Cat# 3176008; RRID: AB_2661813
CD11b (clone ICRF44) 209Bi	Fluidigm	Cat# 3209003; RRID: AB_2687654
Human Fc Receptor Binding Inhibitor	Thermo Fisher Scientific	Cat# 14-9161-73; RRID: AB_468582
Biological Samples		
Whole blood from healthy donors	NIEHS Clinical Research Unit (CRU)	See Table S1 for details
Chemicals, Peptides, and Recombinant Proteins		
Histopaque®-1077	Sigma Millipore	Cat# 10771
ACCUSPIN Tubes	Sigma Millipore	Cat# A2055
Iscove's Modified Dulbecco's Medium (IMDM)	Thermo Fisher Scientific	Cat# 12200036
Fetal Bovine Serum (FBS)	Gemini Bio-Products	Cat# 100-106
autoMACS Running Buffer	Miltenyi Biotec	Cat# 130-091-221
Dimethyl sulfoxide (DMSO)	Millipore Sigma	Cat# D84-18
Ultrapure BSA	Ambion by Life Technologies	Cat# AM2618
Benzonase Nuclease	Millipore Sigma	Cat# E8263-25KU
Phosphate Buffered Saline (PBS)	Thermo Fisher Scientific	Cat# 20012-027
Dynabeads CD15	Thermo Fisher Scientific	Cat# 11137D
Cell-ID Cisplatin-198Pt	Fluidigm	Cat# 201198
Cell-ID Intercalator-Ir—500 μM	Fluidigm	Cat# 201192B

(*Continued on next page*)

Continued

REAGENT or RESOURCE	SOURCE	IDENTIFIER
Maxpar® Cell Staining Buffer	Fluidigm	Cat# 201068
Maxpar® Fix and Perm Buffer	Fluidigm	Cat# 201067
EQ Four Element Calibration Beads	Fluidigm	Cat# 201078
Macron 0754-06 Sodium Citrate, Dihydrate	Thomas Scientific	Cat# 0562N59
SPRIselect Reagent	Beckman Coulter	Cat# B23318
Dynabeads MyOne Silane	Thermo Fisher Scientific	Cat# 37002D
Dynabeads CD19 Pan B	Thermo Fisher Scientific	Cat# 11143D
Dynabeads CD4	Thermo Fisher Scientific	Cat# 11145D
Dynabeads CD8	Thermo Fisher Scientific	Cat# 11147D
Dynabeads CD14	Thermo Fisher Scientific	Cat# 11149D
CD56 MicroBeads, human	Miltenyi Biotec	Cat# 130-050-401
AllPrep DNA/RNA/miRNA Universal Kit	QIAGEN	Cat# 80224
Flowmi™ Tip Strainers	Bel-Art	Cat# H1680-0040
Nuclease-Free Water	Thermo Fisher Scientific	Cat# AM9930
Critical Commercial Assays		
Chromium Single Cell 3′ Library & Gel Bead Kit v2	10X Genomics, Inc.	Cat# 120237
Chromium i7 Multiplex Kit	10X Genomics, Inc.	Cat# 120262
Bioanalyzer High Sensitivity DNA Analysis	Agilent	Cat# 5067-4626
Ovation Pico WTA System V2	NuGEN	Cat# 3302-60
Encore Biotin Module	NuGEN	Cat# 4200-60
GeneChip Hybridization, Wash, and Stain Kit	Thermo Fisher Scientific	Cat# 900720
GeneChip Human Transcriptome Array 2.0	Thermo Fisher Scientific	Cat# 902233
EZ-96 DNA Methylation MagPrep	Zymo Research	Cat# D5041
Infinium HumanMethylation450 BeadChip Kit	Illumina	Cat# WG-314-1002
Infinium MethylationEPIC BeadChip Kit	Illumina	Cat# WG-317-1003
TruSeq Stranded Total RNA Gold	Illumina	Cat# 20020598
Deposited Data		
Single-cell RNA sequencing	This paper	GEO: GSE138867
Bulk RNA sequencing	This paper	GEO: GSE138851
Microarray	This paper	GEO: GSE13897
CD8 T DNA Methylation Array Profiling	This paper	GEO: GSE147430
Flow-sorted CD8 T Microarray	Callender et al.[17]	GEO: GSE98640
Software and Algorithms		
GraphPad Prism 7	GraphPad Software, Inc.	GraphPad Prism,RRID: SCR_002798
Cytobank	Cytobank	https://cytobank.org, RRID: SCR_014043
Transcriptome Analysis Console (TAC)	Thermo Fisher Scientific	Transcriptome Analysis Console, RRID: SCR_016519
VorteX v26	Samusik et al.[14]	https://github.com/nolanlab/vortex, RRID: SCR_017047
CellRanger v2.0.2	10x Genomics	https://support.10xgenomics.com/single-cell-gene-expression/software/pipelines/latest/installation, RRID: SCR_017344
Seurat v3.0.0.9000	Stuart et al.[11]	https://satijalab.org/seurat
Seurat v2.3.4	Butler et al.[10]	https://satijalab.org/seurat
R	R Core	https://www.r-project.org/

(*Continued on next page*)

Continued

REAGENT or RESOURCE	SOURCE	IDENTIFIER
Slingshot v1.2.0	Street et al.[22]	https://bioconductor.org/packages/release/bioc/html/slingshot.html, RRID: SCR_017012
GSEA	Subramanian et al.[83] Mootha et al.[84]	https://www.gsea-msigdb.org/gsea/downloads.jsp, RRID: SCR_003199
GenePattern	Reich et al.[85]	https://www.genepattern.org, RRID: SCR_003201
GEO2R	Barrett et al.[86]	https://www.ncbi.nlm.nih.gov/geo/geo2r/
Minfi	Aryee et al.[87]	bioconductor.org/packages/release/bioc/html/minfi.html
PreprocessNoob	Fortin et al.[88]	https://rdrr.io/bioc/minfi/man/preprocessNoob.html
DNAm PhenoAge	Levine et al.[30]	http://dnamage.genetics.ucla.edu/home
DNAm TL	Lu et al.[31]	http://dnamage.genetics.ucla.edu/home

RESOURCE AVAILABILITY

Lead Contact

Further information and requests for resources and reagents should be directed to and will be fulfilled by the Lead Contact, Dr. Douglas A. Bell (bell1@niehs.nih.gov), Senior Investigator, Environmental Epigenomics and Disease Group, Immunity Inflammation and Disease Laboratory, National Institute of Environmental Health Sciences, Research Triangle Park, NC, USA.

Materials Availability

This study did not generate new unique reagents.

Data and Code Availability

The datasets generated during this study are available at NCBI GEO, https://www.ncbi.nlm.nih.gov/geo/. Microarray data have been deposited to NCBI GEO: GSE138974. Bulk and single-cell RNA-seq data have been deposited to NCBI GEO: GSE138851 and NCBI GEO: GSE138867. Raw idat files for DNA methylation have been deposited to NCBI GEO: GSE147430. Mass cytometry data are available from the corresponding author on request.

EXPERIMENTAL MODEL AND SUBJECT DETAILS

Human Subjects

All donors were recruited with written informed consent under approved human IRB protocol NIEHS 10-E-0063 by the NIEHS Clinical Research Unit between March 2013 to January 2018 from the Raleigh, Durham and Chapel Hill, NC area.[5,6] Whole blood was obtained from healthy (without acute disease according to self-reported medical histories) from nonsmokers, not having smoked > 100 cigarettes in their lifetime, and smokers who reported their average daily cigarette consumption for the past 3 months. Serum nicotine/cotinine levels were measured by HPLC-MS (Quest, Inc.) as an indication of their smoking exposure status. Human cytomegalovirus (HCVM) status was determined by two methods at the NIH Clinical Center in Bethesda, MD. Anti-cytomegalovirus IgG and IgM antibodies were measured in serum by a chemiluminescence immunoassay, and HCMV DNA viral load was determined using CMV-specific probes by quantitative real-time PCR. Donors were recalled matching nonsmokers/smokers on age, gender, and ethnicity for whole blood collection, cotinine levels were measured. See Table S1 for additional donor information.

METHOD DETAILS

PBMC Isolation for scRNA-seq and Mass Cytometry

Whole blood was diluted 1:5 v/v with QIAGEN Buffer EL and incubated at room temperature (RT) until clarified (~10 min) before centrifugation (300 g, RT, 10 min). After supernatant removal, leukocytes were resuspended in the same volume of Buffer EL (5 min) before spinning (300 g, 8 min). Leukocytes were then washed twice in autoMACS Running Buffer (Miltenyi Biotec), counted, and cryopreserved [20% Iscove's Modified Dulbecco's Medium (IMDM), 70% Fetal Bovine Serum (FBS), 10% Dimethyl sulfoxide (DMSO)] at a concentration of $1x10^7$ cells/mL. Cryopreserved cells were thawed in nonsmoker/smoker pairs following the 10X Genomic's protocol for ''Fresh Frozen Human Peripheral Blood Mononuclear Cells for Single Cell RNA Sequencing.'' Briefly, cells were

serially diluted dropwise in complete media (IMDM,10% FBS) adding 50U/mL Benzonase (Millipore Sigma) for the first dilution. After centrifugation (1100 rpm, 8 min, RT), cells were resuspended in complete media and incubated with CD15 Dynabeads (Thermo Fisher Scientific) according to the manufacturer's instructions to deplete the neutrophils from the PBMCs. PBMCs were then counted for viability and aliquoted for scRNA-seq or mass cytometry in parallel.

PBMC Preparation for Purified Cell Fractions

The mononuclear layer was isolated directly from whole blood using density gradient centrifugation with Histopaque-1077 Ficoll and ACCUSPIN Tubes (Sigma Millipore). Purified $CD4^+$, $CD8^+$, $CD14^+$, $CD19^+$, and $CD56^+$ cell fractions were collected using antibody-coated magnetic beads (Dynabeads, Thermo Fisher Scientific; CD56, Miltenyi Biotec). Antibody-purified fractions were then extracted for DNA and RNA using the AllPrep DNA/RNA/miRNA Universal Kit according to the manufacturer's instructions (QIAGEN).

Mass Cytometry

Thawed PBMCs ($\sim 3x10^6$ cells) were spun (300 g, 5 min) and resuspended in calcium magnesium-free phosphate buffered saline (PBS). 1μM Cisplatin (Fluidigm) was added for viability staining for 5 minutes before quenching the reaction with MaxPar Cell Staining Buffer (CSB, Fluidigm). After centrifugation (300 g, 5 min), cells were resuspended in CSB at a concentration of $60x10^6$ cells/mL and incubated (RT,10 min) with Fc receptor binding inhibitor before adding 26 MaxPar metal-conjugated antibodies (Fluidigm) against immunophenotypic markers for an additional 30-minute incubation at RT. Stained cells were then washed two times before resuspension in MaxPar fix and perm buffer with 125μM 191/193Ir intercalator for either an hour at RT or 4°C overnight. Cells were then washed twice with CSB and two times with Nuclease-Free water (Thermo Fisher Scientific) followed by filtering through 40μM strainers to remove aggregates. Cells were then counted and resuspended in nuclease-free water at $\sim 5x10^5$ cells/mL with 1:10 volume of four-element calibration beads (Fluidigm) and analyzed on a Helios instrument (Fluidigm) for 250,000 events for each donor at the NIEHS Flow Cytometry Center. Following the manufacturer's instructions, downstream processing involved normalization by the calibration beads and fcs files were uploaded to Cytobank.

Preparation of Sequencing Libraries

scRNA-seq, libraries were prepared with the Chromium Single Cell 3′ Library & Gel Bead Kit v2 (10X Genomics) according to the manufacturer's guidelines. For bulk RNA-seq, RNA from isolated $CD8^+$ purified cell fractions were prepared using the TruSeq Stranded Total RNA Library Prep Gold (Illumina).

Microarray

Isolated RNA from antibody-purified cell fractions (CD4, CD8, CD14, CD19, CD56) from 19 individuals (9 smokers, 10 nonsmokers (See Table S1)), was amplified using NuGEN WT-Ovation Pico RNA Amplification System followed by labeling with NuGEN Encore Biotin Module according to the manufacturer's protocol (NuGEN). Amplified biotin-cDNA was fragmented and hybridized to streptavidin/phycoerythrin-stained arrays using the GeneChip™ Hybridization, Wash and Stain Kit according to the manual protocol FS450-0004 (Thermo Fisher Scientific). The Life Technologies Human Transcriptome Arrays v2.0 were then scanned by an Affymetrix Scanner 3000 and using Transcriptome Analysis Console (TAC) Software (Thermo Fisher Scientific).

DNA Methylation arrays

Isolated DNA was bisulfite converted using the EZ-96 DNA Methylation MagPrep Kit (Zymo Research). Converted DNA was applied to either an Illumina Infinium HumanMethylation450 BeadChip (450K) or an Infinium MethylationEPIC BeadChip Kit (EPIC) according to the manufacturers' protocol to measure methylation at ~450,000 (450K) or 850,000 (EPIC) CpG sites genome wide.

QUANTIFICATION AND STATISTICAL ANALYSIS

Mass Cytometry Gating Strategy and Analysis

Events were gated in Cytobank to identify single viable cells (Figure S1A). Cells gated from spiked-in normalization beads were subsequently gated by Iridium (191Ir) and Cisplatin (198Pt) to obtain DNA positive cells. Single cells were identified by event length and Iridium (193Ir) and viable cells by Cisplatin-198Pt and leukocyte marker CD45. Viable cells were exported as fcs files and imported into VorteX[14] using all events for each donor totaling 990,748 cells. Using the default parameter recommendations,[89] all data were transformed using hyperbolic arcsin (f = 5). Applying a noise threshold of 1.0, clustering analysis was performed using a Euclidean length profile of 1.0 in X-shift and the weighted K-nearest neighbor density estimation (K). An elbow point validation was performed to determine the optimal cluster K value (K = 25) which was then used to create a Force-Directed Layout (FDL) for visualization colored by major immune cell type, expression of marker genes, cluster ID, smoking status and subject ID (Figures 1C, 1E, S1B, S1C, and S1E). 136 clusters were identified from the 990,748 events, one cluster was determined to be red blood cells (RBCs; positive expression for CD235a/b) and 13 clusters had multiple lineage markers and were determined to be doublets (e.g., positive expression profiles for CD19 and CD3) which was a total of 6900 cells that were removed prior to downstream analysis (983,848 cells retained).

scRNA-seq Processing and Analysis

scRNA-seq data was aligned to the hg19 genome and processed with CellRanger version 2.0.2. Uniquely aligned reads sharing equal barcode × unique molecular identifier (UMI) tags but annotated to multiple protein-coding transcripts (i.e., ambiguous UMIs), within each replicate were discarded from the analysis. Cells with less than 200 or greater than 3000 genes and cells with greater than 10% of UMIs from mitochondria were removed. Dataset integration, SNN clustering, and UMAP visualization of scRNA-seq data were performed with Seurat version 3.0.0.9000.[11] To integrate data across eight donor samples, we used 2,500 genes and 50 dimensions. Clusters were identified by SNN clustering with Seurat FindNeighbors and FindClusters functions using 50 dimensions and a resolution parameter of 2.5. UMAP was used to visualize cells colored by major immune cell type (Figure 1B), cluster ID (Figure 2A), and smoking status (Figure 2B). Cell cluster marker genes ($p_{adj} < 0.05$) and smoking DEGs ($p_{adj} < 0.05$) were identified using Seurat version 2.3.4[10] implementing the MAST algorithm[12] with UMI included as a latent variable. Expression of marker genes were visualized via UMAP (Figure 1D).

Slingshot version 1.2.0[22] was used to perform pseudotime analysis. Principal component analysis and UMAP were run on CD8 T cells using 45 dimensions. Slingshot was then used to infer cluster lineages and assign pseudotime to CD8T cells (Figure 3C). Temporally expressed genes for each CD8 T lineage were then identified by fitting a generalized additive model to each gene using loess-smoothed pseudotime as the predictor variable (Figure S3).

Bulk RNA-seq Analysis

For antibody-purified CD8 T cell fraction bulk RNA-seq, reads were aligned to the hg19 genome with STAR. Gene read counts were obtained with featureCounts from the Subread package using release 27 of the GENCODE annotation. DEGs were determined using DESeq2 with FDR-adjusted p value < 0.05 as the cutoff for significance (Figure 5B). PCA was performed with the prcomp() function in R (Figure 5C).

Microarray Analysis

For microarray, differentially expressed genes were detected using log2-transformed expression fold-change estimates with respect to the composite average of RMA-corrected fluorescence log-intensity levels (log_2FC) across matched fractions (CD14, CD19, CD4, CD56, and CD8) from multiple individual female donors, both smoking and nonsmoking (N = 53 overall, with $N \geq 5$ per cell fraction × smoking status group). Probe-wise log_2FC values were tested across statistical groups through a resolution-weighted ANOVA; resolution weights represented relative metrics of fluorescence discrimination in the dynamic range of detection, i.e., cumulative hazard of multivariate ANOVA significance scores (probe × cell fraction × smoking status) from probe-wise generalized linear modeling of RMA-corrected fluorescence log-intensities using an exponential distribution and inverse link function.[90] DEGs were detected from the annotation of probes with significance level $p < 0.05$ adjusted for multiple comparisons,[91] then filtered against a minimum probe-wise effect size $\delta_{log2FC} > 0.3 \times \sigma_{log2FC}$ and post hoc pairwise significance (Student's t test $p < 0.05$) between log_2FC values of at least one matched comparison between smokers and nonsmokers on same cell fraction levels. For probe-level effect size filtering, $\delta_{log2FC} = 0.3 \times \sigma_{SSR}$ is 5% of the 6σ-spread log_2FC regression error with respect to a probe's grand mean [where $(\sigma_{SSR})^2 = (SSR_{log2FC})/(N-1)$] compared to 5% of the 6σ-spread in measurement error about the mean log_2FC of each statistical group in the probe [where $(\sigma_{log2FC})^2 = (SSE_{log2FC})/(N-1)$].

GSEA

We used GSEA[83,84] via GenePattern[85] to perform gene set enrichment analysis for Chemical and Genetic Perturbations and Immunological Signatures[92] gene sets for scRNaseq, bulk RNA-seq, and microarray using FWER < 0.05 as the cutoff for significant enrichment (Figure 5E).

DNA Methylation Processing and Analysis

The raw idat files from the 450K and EPIC methylation arrays were read into R with the Minfi package separately.[87] Data were combined for common CpG sites on the two arrays with Minfi combineArrays function and then preprocessed with background and dye bias correction using the Noob method.[88] Methylation β values for CpG sites were calculated and values were input into a DNA Methylation Age Calculator[30] to predict epigenetic biomarkers for aging (DNAm PhenoAge) and aging acceleration, determined by the correlation between DNAm PhenoAge and chronological age (DNAm PhenoAgeAccel, Figures 5F and 5H). Telomere length was estimated with DNAmTL[31] (Figures 5G and 5I). Univariable linear regression was used to determine p values for the association of *AHRR* methylation versus DNAm PhenoAgeAccel and DNAmTL.

Reanalysis of Microarray Data

We reanalyzed Callender et al.[17] gene expression data (GSE98640) from isolated CD8 T cells subsets: T_N, T_{CM}, T_{EM};, and T_{EMRA} using GEO2R with default parameters[86] to identify genes with differential expression among CD8 T subsets using limma (Linear Models for Microarray Analysis) with FDR-adjusted p values.[93,94]

Cell Reports Medicine, Volume *1*

Supplemental Information

Single-Cell Analyses Identify Dysfunctional $CD16^{+}$ CD8 T Cells in Smokers

Suzanne N. Martos, Michelle R. Campbell, Oswaldo A. Lozoya, Xuting Wang, Brian D. Bennett, Isabel J.B. Thompson, Ma Wan, Gary S. Pittman, and Douglas A. Bell

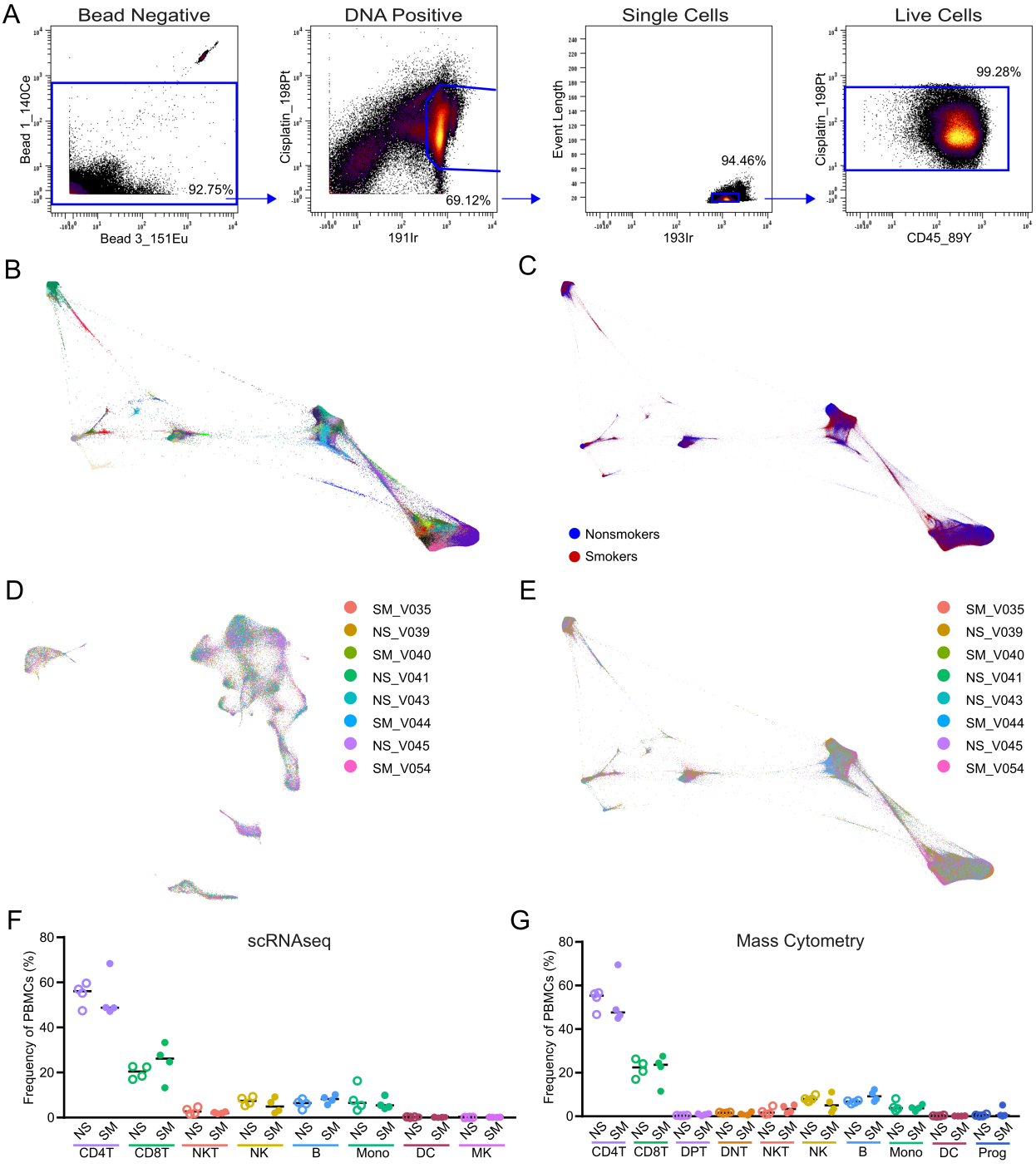

Figure S1. scRNAseq and mass cytometry profiling of PBMCs, Related to Figure 1. (A) Mass cytometry biaxial plots of the gating strategy. Cells gated from spiked-in normalization beads are subsequently gated by Iridium (191Ir) and Cisplatin (198Pt) to obtain DNA positive cells. Single cells are identified by event length and Iridium (193Ir) and viable cells by Cisplatin-198Pt and leukocyte marker CD45 (example from a single donor). **(B-C)** FDL mass cytometry (n=8) of 122 immune cell cluster IDs displayed by cluster ID color **(B)** and smoking status (**C**; 4 nonsmokers blue, 4 smokers red). **(D)** scRNAseq UMAP (n=8) as described in **Figure 1B**. Cells are colored by individual donors. **(E)** Mass cytometry FDL as described in **Figure 1C**. Cells are colored by individual donors. **(F-G)** Frequencies of PBMCs by major cells types compared between smokers (filled, n=4) and nonsmokers (unfilled, n=4) for scRNAseq **(F)** or mass cytometry. **(G)** did not show significant differences. Bar = median, Mann-Whitney U test.

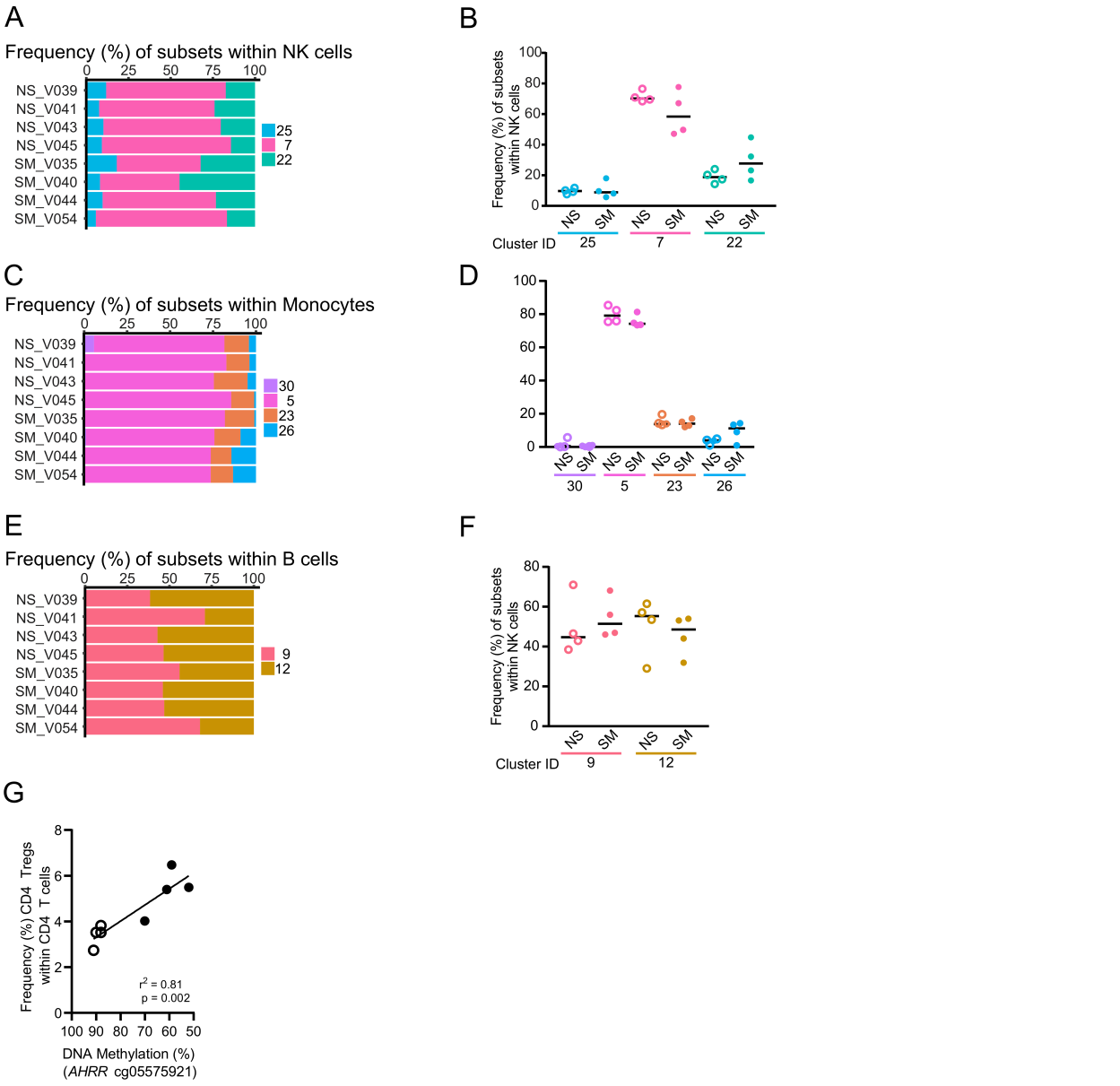

Figure S2. Subtype distributions within other major cell populations do not shift between smokers (SM, n=4) and nonsmokers (NS, n=4), Related to Figure 2. (A-B) Frequency of subsets within NK cells. Individual donor distribution of NK cell subsets **(A)**. Smokers (filled) had no significant shifts in NK cell frequency compared to nonsmokers (unfilled). Bar = median, Mann-Whitney U test **(B)**. **(C-D) Frequency of subsets within monocytes.** Individual donor distribution of monocyte subsets **(C)**. Smokers (filled) had no significant shifts in monocyte frequency compared to nonsmokers (unfilled). Bar = median, Mann-Whitney U test **(D)**. **(E-F) Frequency of subsets within B cells.** Individual donor distribution of B cell subsets **(E)**. Smokers (filled) had no significant shifts in B cell frequency compared to nonsmokers (unfilled). Bar = median, Mann-Whitney U test **(F)**. **(G)** Frequency of CD4 Tregs correlated with smoking dose (reduced *AHRR* DNA methylation).

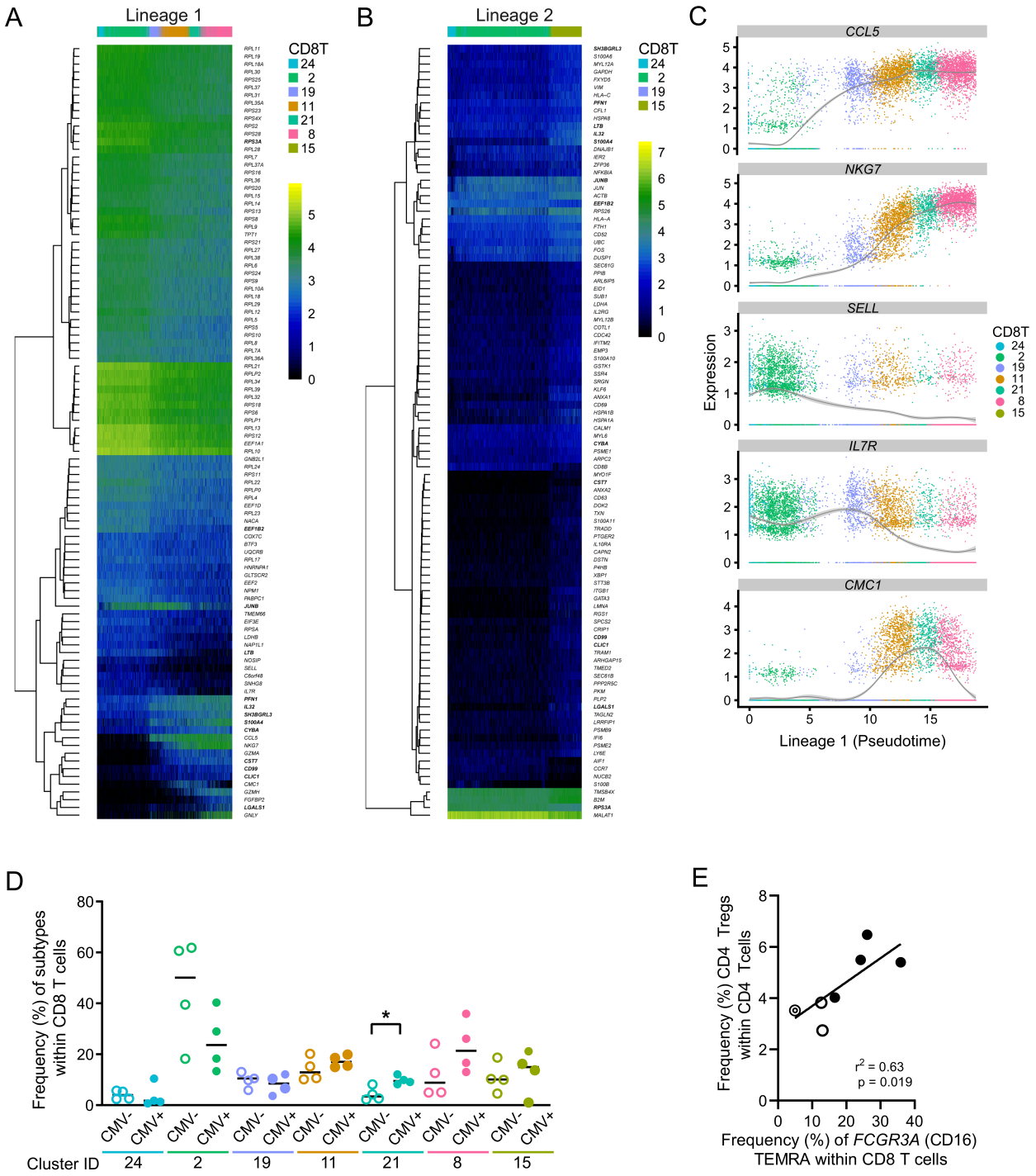

Figure S3. CD8 subsets shift from naïve to differentiated CD8 T cell states, Related to Figure 3.
(A-B) Pseudotemporal heatmaps of CD8 T cell differentiation (n=8) of Lineage 1 **(A)** and Lineage 2 **(B)**.
(C) Pseudotemporal trajectory of CD8 T cell differentiation in Lineage 1 of *CCL5*, *NKG7*, *SELL*, *IL7R* and *CMC1*.
(D) Human cytomegalovirus (HCMV) seropositive (IgG+/IgM-) donors (filled, n=4) had significantly increased frequency of CD8T-21 cells compared to HCMV seronegative (IgG-/IgM-) donors (unfilled, n=4). Bar=median, *p<0.05 by Mann-Whitney U test. **(E)** Frequency of CD4 Tregs correlated with frequency of *FCGR3A* CD8 T_{EMRA} cells.

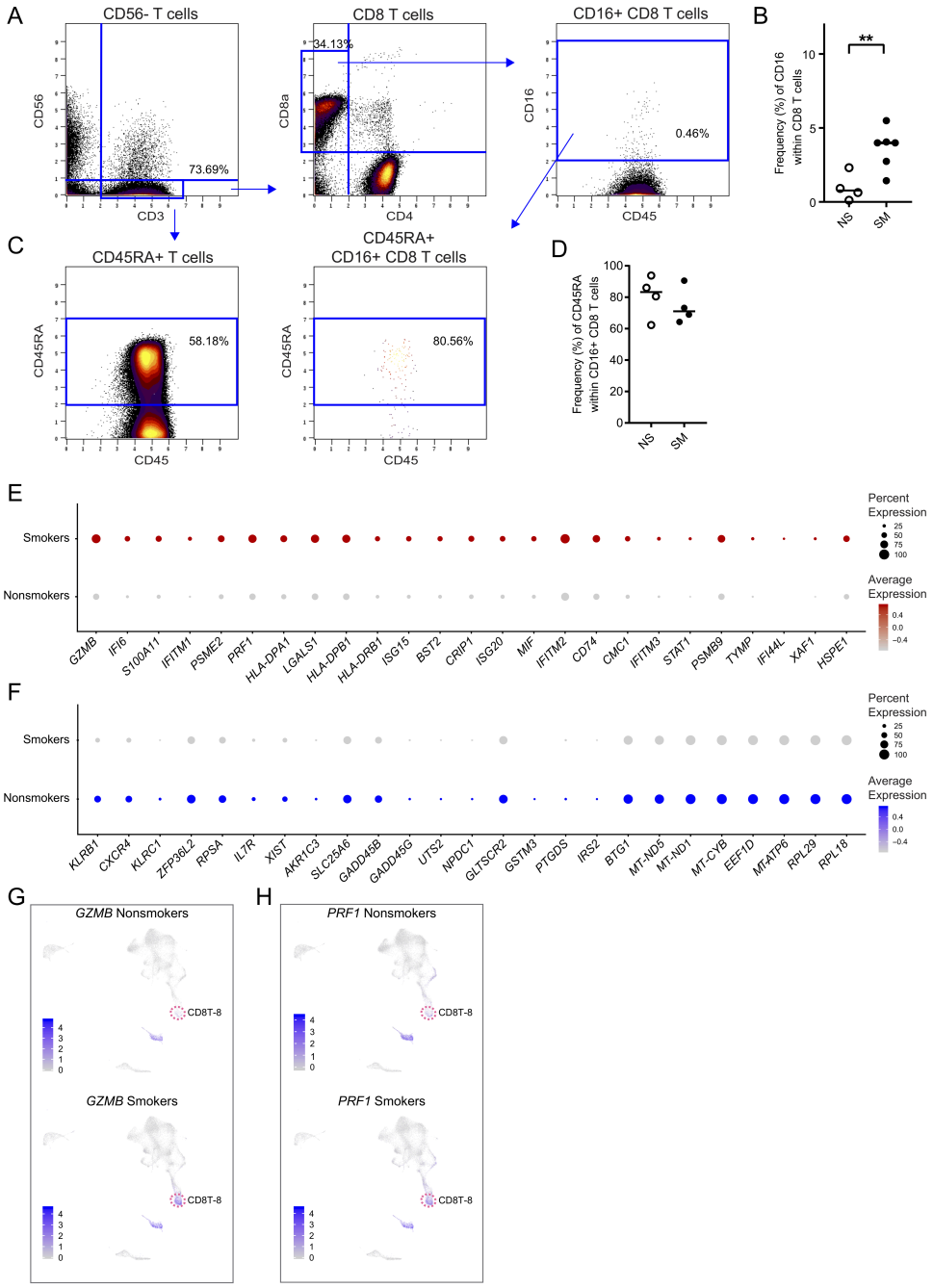

Figure S4. CD16$^+$ CD8 T cells characterization by scRNAseq, Related to Figure 4. (A) Mass cytometry gated to determine frequency of CD16$^+$ CD8 T cells (example from single donor). Viable cells (**Figure S1A**, right panel) in a CD3/CD56 biaxial plot. CD56$^-$ cells (lower right quadrant) gated by CD4 and CD8 to obtain single positive CD8 T cells (upper left quadrant) were used to determine CD16$^+$ CD8 T cell frequency. **(B)** CD16$^+$ cells increased in smokers' CD8 T cells (filled, n=6) compared to nonsmokers (unfilled, n=4) in an independent group of donors. Bar=median, **p<0.01 by one-tailed Mann-Whitney U test. **(C)** CD3$^+$ T cells gated by CD45RA/CD45 to establish CD45RA$^+$ gate and applied to CD16$^+$ CD8 T cells showed the majority were CD45RA positive. **(D)** CD45RA$^+$ cell frequency in CD16$^+$ CD8 T cells from smokers (n=4) and nonsmokers (n=4). Bar = median, Mann-Whitney U test. **(E-F)** Genes altered in smokers in the CD8T-8 subset. 25 genes with increased **(E)** or decreased **(F)** per cell gene expression were ordered by the difference in percentage of CD8T-8 cells expressing each gene between smokers (n=4) and nonsmokers (n=4). Color intensity indicates average per cell expression and circle size represents percent of cells expressing the gene. **(G-H)** UMAP comparison of nonsmokers and smokers, as described in **Figure 4C** and **4E,** displaying the increase in *GZMB* **(G)** and *PRF1* **(H)** from smokers in the CD8T-8 cluster.

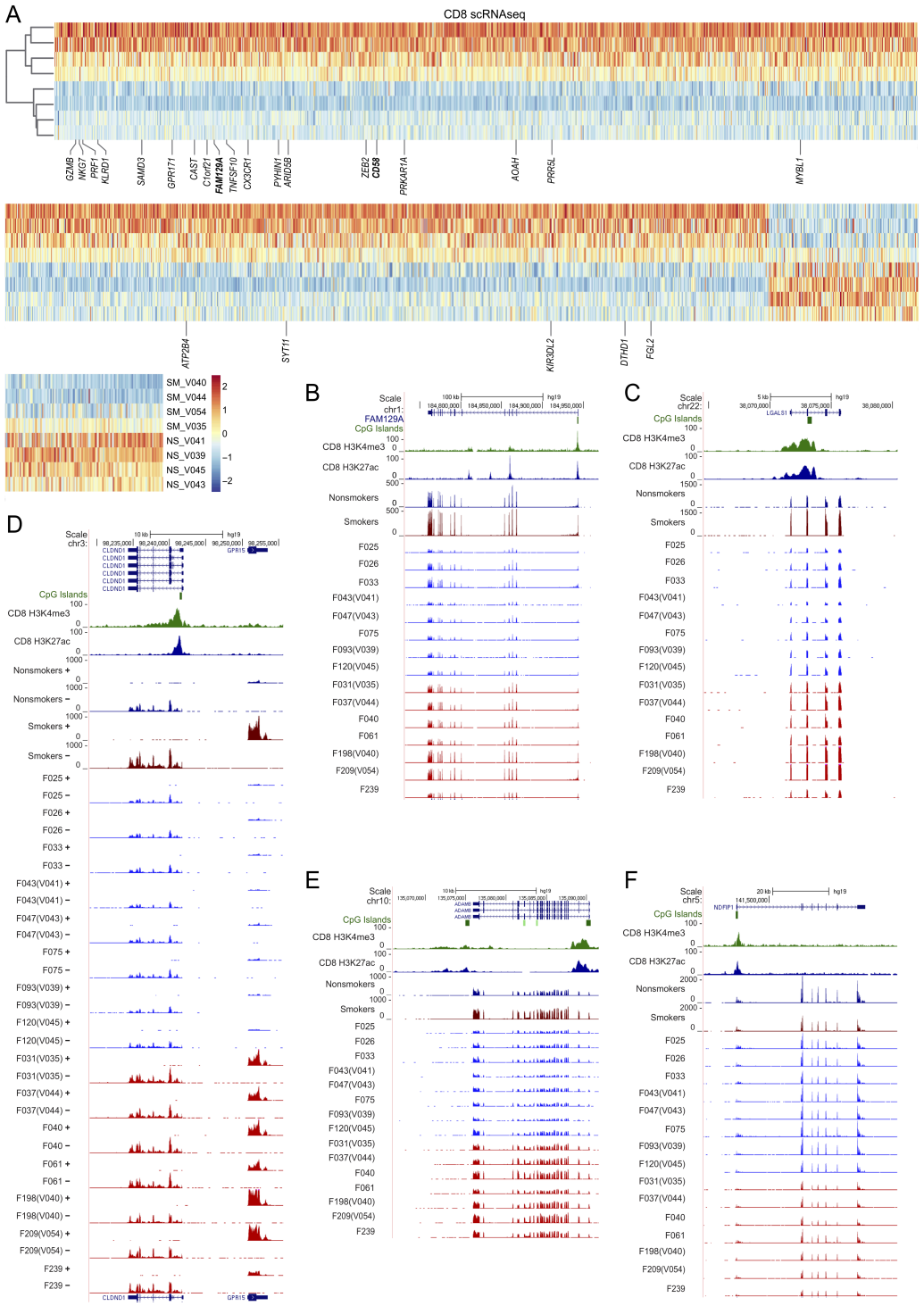

Figure S5. Activation of CD8 T cells in peripheral blood of smokers, Related to Figure 5. (A) scRNAseq heatmap of all differentially expressed genes (DEGs) between smokers (n=4) and nonsmokers (n=4) from seven CD8 T cells clusters. Individual donors were separated by smoking status using smoking scRNA-DEGs for hierarchical clustering. Genes labeled were also found to be significantly upregulated in the CD8 T cell microarray results (See **Figure 5D**). **(B-F) Genome browser tracks of DEGs from bulk RNAseq (n=8 nonsmokers, n=7 smokers).** *FAM129A* was significantly increased by all three platforms **(B)**. *LGALS1* **(C)**, *CLDND1* **(D)**, and *ADAM8* **(E)**, were significantly increased in bulk RNAseq and scRNAseq data, while *GPR15* **(D)** was increased in RNAseq and microarray data. *NDFIP1* **(F)** was significantly decreased in bulk RNAseq and scRNAseq data.

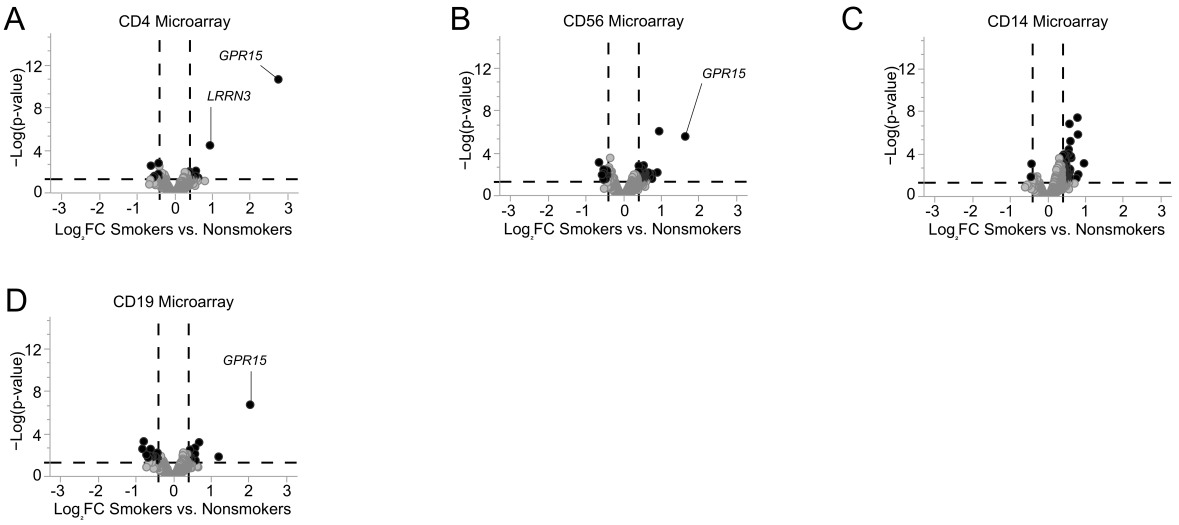

Figure S6. Other major cell type expression changes in peripheral blood of smokers, Related to Figure 6. **(A-D)** Microarray volcano plots of isolated $CD4^+$ T cells **(A,** n=10 nonsmokers, n=9 smokers**)**, $CD56^+$ cells **(B,** n=11 nonsmokers, n=12 smokers**)**, $CD14^+$ cells **(C,** n=10 nonsmokers, n=9 smokers**)** and $CD19^+$ B cells **(D,** n=10 nonsmokers, n=9 smokers**)**.